Chapter 5

Dielectric waveguides

Contents

5.1 Introduction

During the last decade, the application of complex optical systems has enormously grown. These systems are applied in such different areas as optical fiber telecommunication, optical datacom, optical data storage (CD-ROM,DVD, Blue-Ray), sensors, printers and many more. Classical optical systems consist of a collection of separate optical components (lenses, mirrors, diffractive elements, light sources, light detectors), which are carefully assembled together. Typically all components need to be aligned very accurately with respect to each other, which makes these systems large, less robust and expensive. In the same way as electronics evolved from discrete components on printed circuit boards to monolithic integrated circuits, also in optics a miniaturization and integration process is ongoing however. The idea of integrated optics was introduced in the late 60s and comprises the integration of different optical functionalities onto a single substrate. To route the light through the components, optical waveguides are used instead of free space propagation. In the early days of integrated optics, most activities were focused on the development of single components, both passive (couplers, filters) and active (lasers, detectors). Later focus shifted towards bringing these different functions together on a single chip. This led to state-of-the-art components consisting of a combination of different complicated subcomponents. A typical example demonstrating the strength of optical integration is shown in figure 5.1. The left picture shows a fiber-based 4-channel 2x2 cross-connect module while the right picture shows an integrated device with the same functionality. It is obvious that the latter has a size several orders

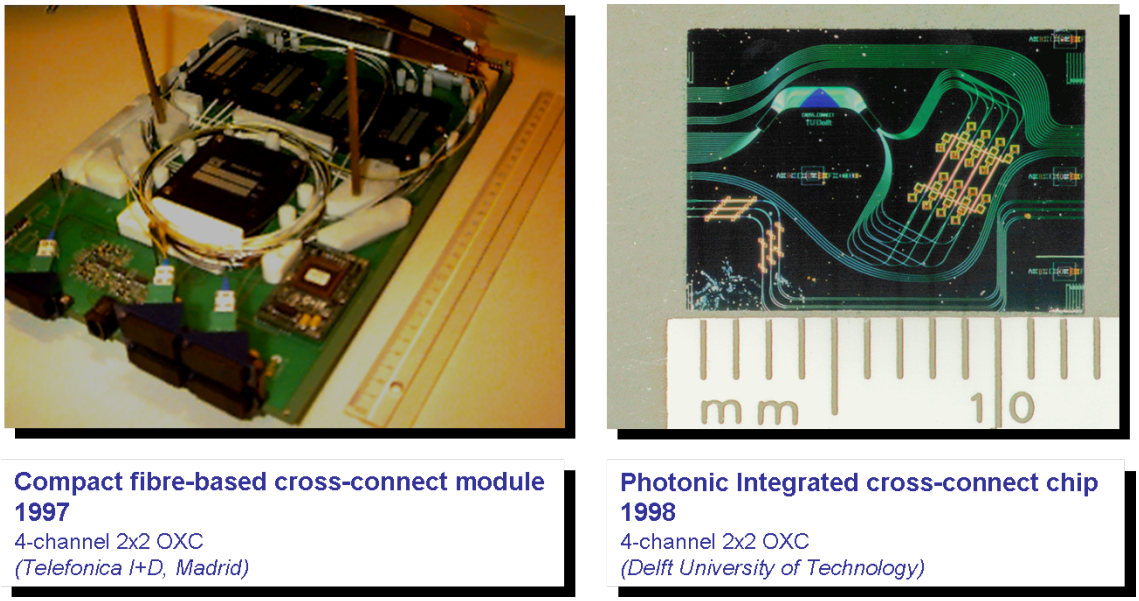

Figure 5.1: Left: compact fiber-based 4-channel 2x2 cross-connect module (Telefonica I&D, Madrid). Right: Photonic integrated 4-channel 2x2 cross-connect module (Cobra Institute, TU/e)

of magnitude smaller than the discrete device. This type of complex integrated components is currently in a research phase but there is a rapid evolution towards commercial applications.

The fundamental idea behind integrated optics is the manipulation of light by waveguides and not by free space optical components like lenses and mirrors. The optical field is guided by dielectric waveguide structures, which is possible because light prefers to be concentrated in the area with the highest refractive index. Figure 5.2 represents different types of waveguides that are used in integrated optics. The optical field will always be located in the area with the highest average refractive index.

The depicted waveguide structures can be realized in different material systems. Each material system has its own advantages and drawbacks. So for every specific application one will have to make a well-considered decision for a given material system. Below the properties of some important material systems are listed.

- InGaAsP/InP

  This crystalline semiconductor material allows for monolithic integration, being the integration of laser diodes and photodiodes together with passive components. This can be done in the $1.3\mu m$ and $1.5\mu m$ wavelength range where the optical fiber has the lowest loss. Waveguides are formed by epitaxial layer growth on an InP substrate and by etching. Due to the high refractive index and the high index contrasts, waveguide structures typically are small (order 1-$2\mu m$), which can lead to problems when coupling light from an optical fiber into the waveguide.

- AlGaAs/GaAs

  This crystalline semiconductor material allows for monolithic integration in the $0.8\mu m$ wavelength range. The corresponding components are mostly used for short distance communi-

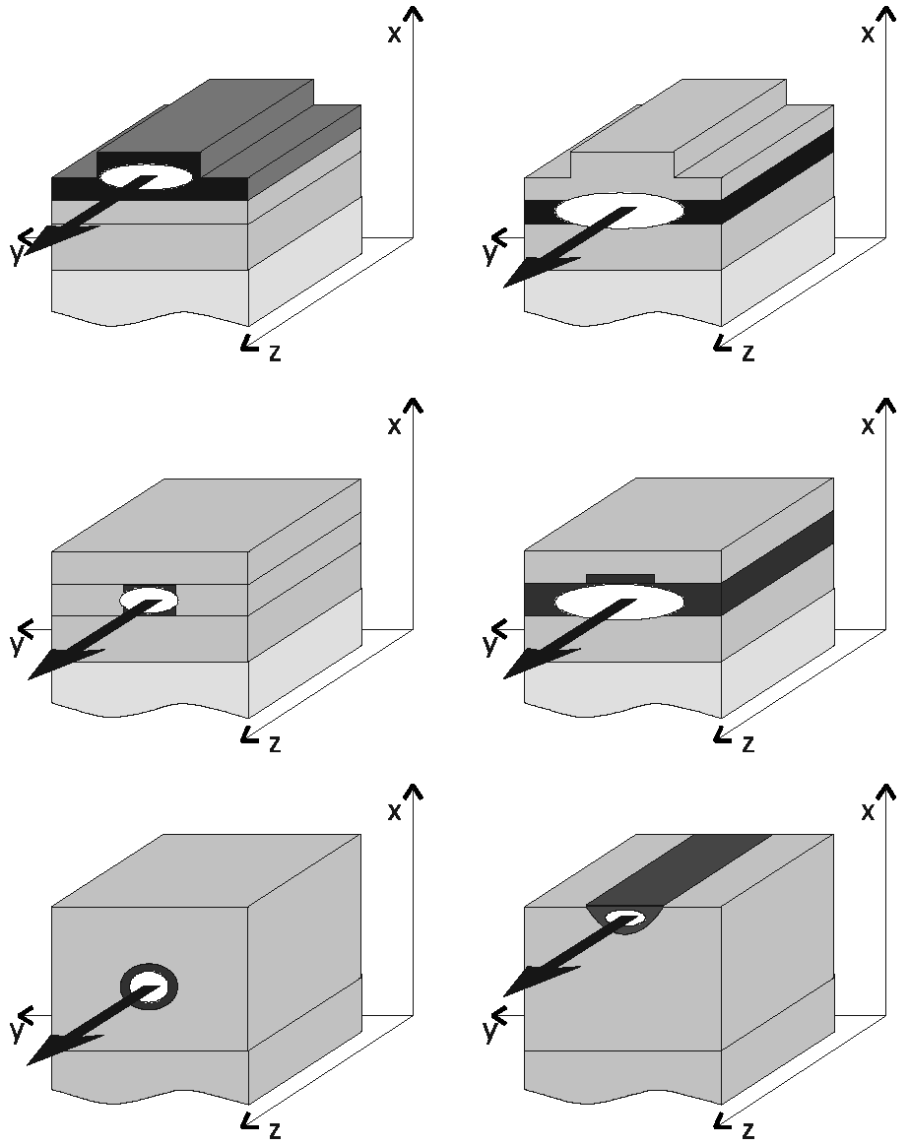

Figure 5.2: Different waveguide structures

cation, in scanners and in CD-players. The same remarks as in the InP/InGaAsP material system concerning coupling to an optical fiber hold.

- Glass

  Waveguides in glass are fabricated using two different types of technologies: diffusion and deposition. The first technique is based on the ion exchange process in special types of glasses by pure thermal or field assisted diffusion. The second technique is based on the deposition of glass (Silica or SiO2) by means of chemical vapour deposition (CVD) or flame hydrolysis (FHD) on a substrate, mostly Silicon. The large waveguide cross-section allows easy coupling with optical fibers. These are currently the preferred methods for fabricating passive optical integrated circuits. Because of the low index contrast, devices are relatively big however.

- $LiNbO_3$

  Lithium niobate is an anisotropic crystalline material with strong electro-optical and acousto-optical properties. Waveguides are fabricated using a diffusion process. Due to the anisotropy components always show a large polarization dependence. The electro-optical effect is used to realize efficient optical switches.

- Polymers

  Polymers represent a broad set of materials. For purely passive applications polycarbonate (also used for compact disks) and PMMA are the preferred materials. Other types of polymers show a large electro-optical or non-linear coefficient but this is mostly at the expense of a reduced long term stability.

- Silicon-on-Insulator

  Waveguides are fabricated in a Silicon layer (high refractive index), which is bonded on a Silicon wafer via an intermediary silica layer (low refractive index). SOI waveguides exist in two different varieties with very different properties: "fiber matched" (typical dimensions around $7\mu m$) and high-contrast (typical dimensions 500nm). The advantage of using Silicon-on-Insulator is that standard CMOS technology can be used to fabricate the waveguides. Even CMOS-electronics and optical circuits can be combined on the same substrate. The high-contrast waveguides open the way to very large scale integrated optics.

For a long time, III-V technologies were thought to push aside other technologies because they were the only ones allowing for monolithic integration. But due to the complicated fabrication process, the high cost, the high fiber to chip coupling losses and the high propagation losses of III-V waveguides, different material systems tend to co-exist, each used for their specific application. The chart below gives an overview of the most important properties of the materials discussed here (T: Telecom / I: Interconnect).

	InP	GaAs	Glass	LiNbO3	Polymers	SOI
Transmitters/Receivers	Yes	Yes	No	No	No	No
Passive optics	Yes	Yes	Yes	Yes	Yes	Yes
Wavelength range	T	I	T,I	T,I	T,I	T
Fiber to chip coupling loss	>2	>2	0.4	<1	<0.5	1
Propagation losses (dB/cm)	2	2	<0.1	<0.3	0.1-1.5	2
$\mathrm{d}n/\mathrm{d}T$ $[10^{-4}/\mathrm{K}]$	1.8	2.5	<0.1	<0.1	0.1-1.5	1.7
$\lvert n_{\mathrm{TE}} - n_{\mathrm{TM}}\rvert$ $[10^{-4}]$	0.1-10	2-10	0.1-0.5	400	2-50	0.1-...
long term stability	+	+	+	+	?	+
wafer dimensions	2-3 inch	3 inch	$\geq$ 4 inch	3 inch	$\geq$ 8 inch	8-12 inch

Fiber to chip coupling losses can be improved by the use of tapers.

5.2 Modes of Optical Waveguides

5.2.1 Introduction

The starting point for the theoretical treatment of the interaction of light and dielectric structures are Maxwells equations. We only assume isotropic and non-magnetic media and a harmonic time dependence of $e^{j\omega t}$. In this case, and in the absence of sources and currents, we can write Maxwells equations as (see also chapter 2):

$$\begin{aligned}
&\nabla \times \mathbf{E}(x,y,z) = -j\omega\mu_0\mathbf{H}(x,y,z)\\
&\nabla \times \mathbf{H}(x,y,z) = j\omega\varepsilon(x,y,z)\mathbf{E}(x,y,z)\\
&\nabla \cdot (\varepsilon(x,y,z)\mathbf{E}(x,y,z)) = 0\\
&\nabla \cdot \mathbf{H}(x,y,z) = 0
\end{aligned} \tag{5.1}$$

In these equations the constitutive relations

$$\begin{aligned}
&\mathbf{D} = \varepsilon\mathbf{E} = \varepsilon_0 n^2\mathbf{E}\\
&\mathbf{B} = \mu_0\mathbf{H}
\end{aligned} \tag{5.2}$$

are implicitly assumed. The real part of the refractive index profile $n(x,y,z,\omega)$ relates the wavelength inside the medium $\lambda = \frac{\lambda_0}{\mathrm{Re}(n)}$ and the vacuum wavelength λ_0. The imaginary part of the refractive index describes the absorption (or gain) of the optical field.

Based on the Maxwells curl equations, vectorial wave equations for the electric field **E** and magnetic field **H** can be written as

$$\begin{aligned}
&\nabla^2\mathbf{E}(\mathbf{r}) + \nabla(\tfrac{\nabla n^2(\mathbf{r})}{n^2(\mathbf{r})}\mathbf{E}(\mathbf{r})) + k_0^2 n^2(\mathbf{r})\mathbf{E}(\mathbf{r}) = 0\\
&\nabla^2\mathbf{H}(\mathbf{r}) + \tfrac{\nabla n^2(\mathbf{r})}{n^2(\mathbf{r})} \times (\nabla \times \mathbf{H}(\mathbf{r})) + k_0^2 n^2(\mathbf{r})\mathbf{H}(\mathbf{r}) = 0
\end{aligned} \tag{5.3}$$

In these equations the gradient of the refractive index occurs, which couples the three components of the field vector. When the refractive index is piecewise constant however, or if the variation of the refractive index is small, we can neglect these gradients so both vectorial equations (5.3)

decouple and reduce to the Helmholtz equation for every component of the field vector (both electric and magnetic field)

$$\nabla^2\Psi(\mathbf{r}) + k_0^2 n^2(\mathbf{r})\Psi(\mathbf{r}) = 0 \tag{5.4}$$

For the further study of optical waveguides, the boundary conditions at the interface between two isotropic materials with dielectric constants ε_1 and ε_2 are important. These are:

$$\begin{aligned} &n \times (\mathbf{E}_1 - \mathbf{E}_2) = 0 \\ &n \times (\mathbf{H}_1 - \mathbf{H}_2) = 0 \\ &n \cdot (\varepsilon_1\mathbf{E}_1 - \varepsilon_2\mathbf{E}_2) = 0 \\ &n \cdot (\mathbf{H}_1 - \mathbf{H}_2) = 0 \end{aligned} \tag{5.5}$$

, which means that the tangential components of the electric and the magnetic field and the normal component of the magnetic field are continuous at an interface. The normal component of the electric field is discontinuous at an interface.

By applying these boundary conditions the field components will in general be related (although they seemed to be uncoupled by neglecting the refractive index gradient terms in equation (5.3)). Note that it is often sufficient to apply the boundary conditions for the tangential components because then automatically the boundary conditions for the normal components are met.

The general solution of Maxwells equations for an arbitrary dielectric structure $\varepsilon(x, y, z)$ requires the solution of a complex set of partial differential equations and requires a lot of computation power. Therefore, in the early days of integrated optics, a lot of effort was put in the development of acceptable approximated calculation methods. A typical example is the effective index method. As more powerful computers became available, numerical methods like finite differences and finite elements methods were used for the analysis of waveguide structures. Nevertheless, approximated solutions in general and the effective index method in particular remain very important design and modeling tools. Some of the methods will be described later in this chapter.

5.2.2 Modes of longitudinally invariant dielectric waveguide structures

In this section we will consider waveguide structures that are invariant in the propagation direction of the optical power. A typical example is shown in figure 5.3. When we choose the z-direction as the propagation direction we can write the refractive index profile as $n(\mathbf{r}) = n(x, y)$

An eigenmode of the waveguide structure is a propagating or evanescent wave of which the transversal shape does not change during propagation. An eigenmode propagating in the positive z-direction is represented by

$$\begin{aligned} \mathbf{E}(\mathbf{r}) &= \mathbf{e}(x, y)e^{-j\beta z} \\ \mathbf{H}(\mathbf{r}) &= \mathbf{h}(x, y)e^{-j\beta z} \end{aligned} \tag{5.6}$$

Three different parameters can be used to describe the propagation characteristics of the eigenmode. The first parameter is the propagation constant β, the second is the effective refractive index

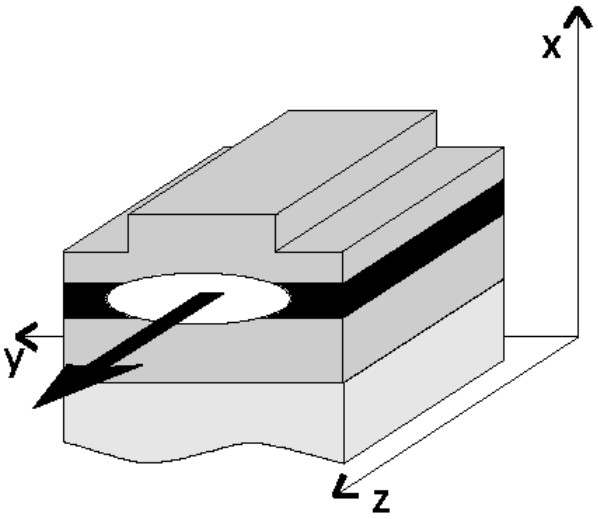

Figure 5.3: Longitudinally invariant waveguide

$$n_{eff} = \frac{\beta}{k_0} \tag{5.7}$$

and the third parameter is the effective dielectric constant

$$\varepsilon_{eff} = n_{eff}^2 \tag{5.8}$$

In the following section we will show that this is the eigenvalue of the eigenvalue equation resulting from Maxwells equations and for which the eigenmodes are the solutions we are looking for. Before we continue with a detailed analysis of the eigenvalue problem, we will first list some important properties of lossless optical waveguides, namely waveguides for which

$$\mathrm{Im}(\varepsilon(x, y)) = 0 \tag{5.9}$$

Figure 5.4 shows the dielectric profile of a hypothetic waveguide together with different eigenmodes of the structure. Theoretically one can show that

1. There are no eigenmodes with an eigenvalue larger than the maximum of the dielectric function.

$$\varepsilon_{eff} < \max(\varepsilon(\mathbf{r}_t)) \tag{5.10}$$

2. Guided modes belong to a discrete set of eigenvalues. These are in the range

$$\varepsilon_{\max} > \varepsilon_{eff} > \max(\varepsilon_{clad}) \tag{5.11}$$

   For these modes

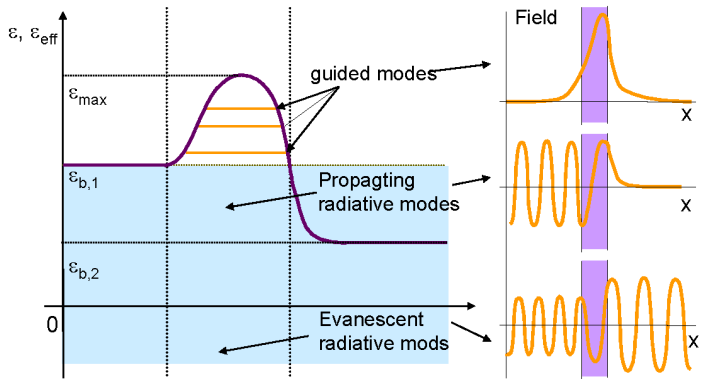

Figure 5.4: Eigenmodes in an optical waveguide

$$\lim_{|\mathbf{r}_t|\to\infty} \Psi(\mathbf{r}_t) = 0 \tag{5.12}$$

Note that there are waveguide structures that do not support a guided mode.

3. The continuous part of the spectrum is formed by the radiating modes for which the eigenvalues

$$\varepsilon_{eff} < \max(\varepsilon_{clad}) \tag{5.13}$$

Radiating modes show an oscillating behaviour along at least one side of the waveguide structure. Depending on their effective refractive index they are classified as propagating or evanescent radiating modes. In the last case the effective refractive index is purely imaginary.

4. Guided and radiating modes form a complete set of functions. This means that every field inside the waveguide can be represented by a sum of these modes:

$$\mathbf{E}(x,y,z) = \sum_m a_m \mathbf{e}_m(x,y) e^{-j\beta_m z} + \int a(k)\mathbf{e}_k(x,y)e^{-jkz}dk \tag{5.14}$$

In this equation we can see the discrete sum of the guided modes and the continuous spectrum of radiating modes.

Note that a radiating mode can be associated with a plane wave incident from the side (figure 5.5).

5.2.3 The slab waveguide

A further simplification to analyze waveguide structures is to consider waveguide structures that are not only invariant in the propagation direction but also in the direction perpendicular to the

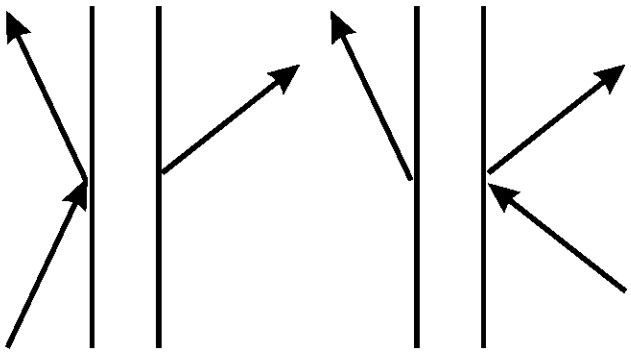

Figure 5.5: Radiating mode

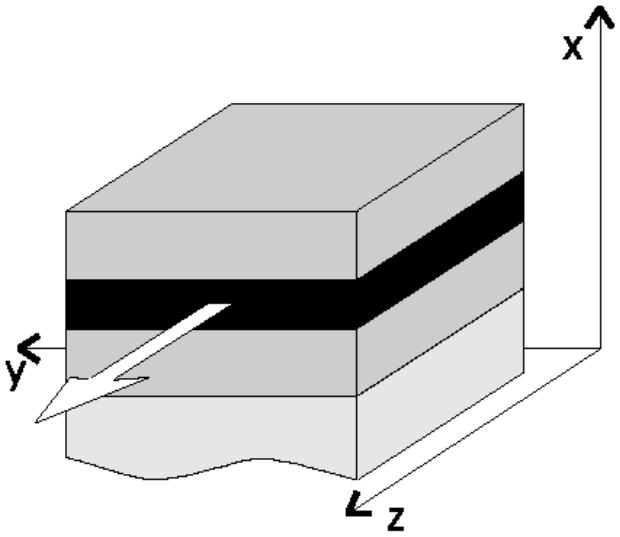

Figure 5.6: Slab waveguide

propagation direction as shown in figure 5.6. These slab waveguides are in practice hardly used but their analysis is the starting point of many approximated theories and so called slab solvers are the basis of many simulation tools for optical waveguides.

We can rewrite equation (5.6) as

$$\begin{aligned} \mathbf{E}(\mathbf{r}) &= \mathbf{e}(x)e^{-j\beta z} \\ \mathbf{H}(\mathbf{r}) &= \mathbf{h}(x)e^{-j\beta z} \end{aligned} \tag{5.15}$$

Substituting these equations in Maxwells curl equations leads to two sets of equations for the so called transverse electric (TE) and transverse magnetic eigenmodes, characterized by the field components $e_y(x), h_x(x), h_z(x)$ and $h_y(x), e_x(x), e_z(x)$ respectively:

$$
\begin{aligned}
TE &\begin{cases} \beta e_y(x) = -\omega\mu_0 h_x(x) \\ \frac{de_y(x)}{dx} = -j\omega\mu_0 h_z(x) \\ \omega_0\varepsilon_0 n^2(x) e_y(x) = -\beta h_x(x) + j\frac{dh_z(x)}{dx} \end{cases} \\
TM &\begin{cases} \beta h_y(x) = \omega\varepsilon_0 n^2(x) e_x(x) \\ \frac{dh_y(x)}{dx} = j\omega\varepsilon_0 n^2(x) e_z(x) \\ \omega\mu_0 h_y(x) = \beta e_x(x) - j\frac{de_z(x)}{dx} \end{cases}
\end{aligned}
\tag{5.16}
$$

in which $\varepsilon_r(x)$ is replaced by $n^2(x)$. By eliminating the x and z field components we can derive a second order differential equation for $e_y(x)$ and $h_y(x)$ respectively:

$$
\begin{aligned}
&\frac{d^2 e_y(x)}{dx^2} + k_0^2 n^2(x) e_y(x) = \beta^2 e_y(x) \\
&\frac{d}{dx}\left(\frac{1}{k_0^2 n^2(x)}\frac{dh_y(x)}{dx}\right) + h_y(x) = \frac{\beta^2}{k_0^2 n^2(x)} h_y(x)
\end{aligned}
\tag{5.17}
$$

An important type of slab waveguide is the so called multi layer slab waveguide. This waveguide consists of a number of layers with refractive index n_i. Because the refractive index is piecewise constant in the multi layer slab waveguide, we can rewrite equations 5.17 as

$$
\begin{aligned}
&\frac{d^2 e_{y,i}(x)}{dx^2} + k_0^2 n_i^2 e_{y,i}(x) = \beta^2 e_{y,i}(x) \\
&\frac{d}{dx}\left(\frac{1}{k_0^2 n_i^2}\frac{dh_{y,i}(x)}{dx}\right) + h_{y,i}(x) = \frac{\beta^2}{k_0^2 n_i^2} h_{y,i}(x)
\end{aligned}
\tag{5.18}
$$

and the TE and TM equations become identical. Solutions will be different however because of the different boundary conditions for TE and TM field components at the interfaces between the different layers. We will continue to work with the TE equation, in order not to overload the notation. The analysis for the TM equation is similar.

The general solution to equation 5.18 can be written as

$$
e_{y,i} = A_i e^{jk_{x,i}(x-a_i)} + B_i e^{-jk_{x,i}(x-a_i)} \tag{5.19}
$$

with

$$
k_{x,i} = \sqrt{k_0^2 n_i^2 - \beta^2} \tag{5.20}
$$

The used notations are clarified in figure 5.7.

Based on equations 5.5 we can derive the following boundary conditions for the interface between two layers:

$$
\begin{cases} e_{y,i}(a_i) = e_{y,i+1}(a_i) \\ \frac{de_{y,i}(a_i)}{dx} = \frac{de_{y,i+1}(a_i)}{dx} \end{cases} \tag{5.21}
$$

apply. Using equations 5.21 and 5.19 we can derive the following matrix relation:

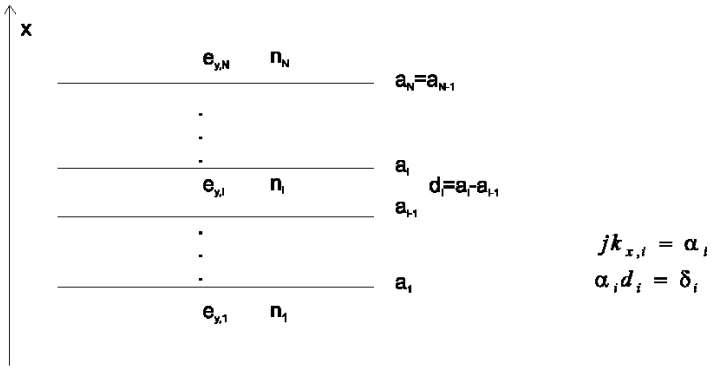

Figure 5.7: Multi layer slab waveguides

$$\begin{bmatrix} A_i \\ B_i \end{bmatrix} = \frac{1}{2\alpha_i} \begin{bmatrix} (\alpha_i + \alpha_{i+1})e^{-\delta_{i+1}} & (\alpha_i - \alpha_{i+1})e^{\delta_{i+1}} \\ (\alpha_i - \alpha_{i+1})e^{-\delta_{i+1}} & (\alpha_i + \alpha_{i+1})e^{\delta_{i+1}} \end{bmatrix} \begin{bmatrix} A_{i+1} \\ B_{i+1} \end{bmatrix} \tag{5.22}$$

By repeating this procedure for all layers, the following matrix equation can be derived:

$$\begin{bmatrix} A_1 \\ B_1 \end{bmatrix} = \begin{bmatrix} t_{11}(\beta^2) & t_{12}(\beta^2) \\ t_{21}(\beta^2) & t_{22}(\beta^2) \end{bmatrix} \begin{bmatrix} A_N \\ B_N \end{bmatrix} \tag{5.23}$$

For guided modes

$$\lim_{x \to \pm\infty} e_y(x) = 0 \tag{5.24}$$

and because $\beta > k_0 n_N$ and $\beta > k_0 n_1$ we can write that $A_1 = B_N = 0$ (if we choose $+j$ as the solution to $\sqrt{-1}$). From equation 5.23 we can see that this can only be fulfilled if $t_{11}(\beta^2) = 0$. The solutions to this dispersion equation yield the guided modes of the structure. Note that this matrix description actually is identical to the analysis for the reflection and transmission of a plane wave at a layer stack discussed in the previous chapter.

Finding the solutions to the dispersion equation has to be done numerically. Only in the case of a 3-layer slab waveguide some interesting properties can be derived analytically.

In the case of a 3-layer slab waveguide, equation 5.19 can be written as (with the notations as depicted in figure 5.2.3)

$$\begin{cases} e_y = Ae^{-\delta x} & (x \geq 0) \\ e_y = A\cos(\kappa x) + B\sin(\kappa x) & (-d \leq x \leq 0) \\ e_y = (A\cos(\kappa d) - B\sin(\kappa d))e^{\gamma(x+d)} & (x \leq -d) \end{cases} \tag{5.25}$$

With

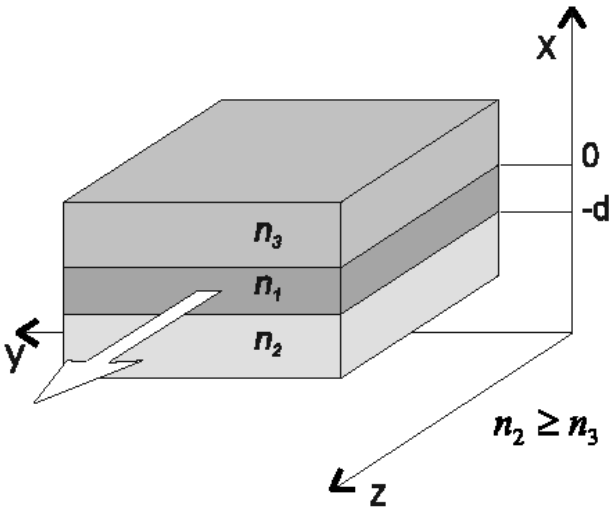

Figure 5.8: Three layer slab waveguide

$$\begin{aligned} \delta &= \sqrt{\beta^2 - n_3^2 k_0^2} \\ \kappa &= \sqrt{n_1^2 k_0^2 - \beta^2} \\ \gamma &= \sqrt{\beta^2 - n_2^2 k_0^2} \end{aligned} \tag{5.26}$$

Hereby we already used the first of the boundary conditions (5.21). To determine A and B we also have to apply the second boundary condition of (5.21). In this way we find following transcendental equation (for TE slab modes):

$$\tan(\kappa d) = \frac{\kappa(\gamma + \delta)}{\kappa^2 - \gamma\delta} \tag{5.27}$$

This is an eigenvalue equation for β with discrete solutions.

For TM slab modes one can find that this transcendental equation can be written as

$$\tan(\kappa d) = \frac{\kappa(\gamma \frac{n_1^2}{n_2^2} + \delta \frac{n_1^2}{n_3^2})}{\kappa^2 - \gamma \frac{n_1^2}{n_2^2} \delta \frac{n_1^2}{n_3^2}} \tag{5.28}$$

With each eigenvalue β an eigenmode can be associated. Often an ω-β diagram is used, being the graphical representation of the dispersion relation for the different eigenmodes. To get a graph (i.e. for the TE polarized slab modes), which is generic, a number of normalized units are used: the normalized frequency ν, the relative effective index b and the asymmetry factor a_{TE}. These are defined as:

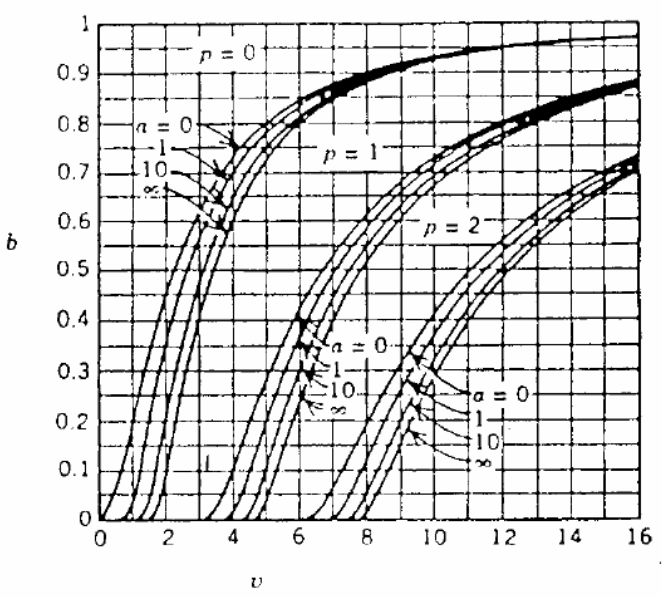

Figure 5.9: Waveguide dispersion curves

$$\begin{aligned} \nu &= k_0 d\sqrt{n_1^2 - n_2^2} \\ b &= \frac{n_{eff}^2 - n_2^2}{n_1^2 - n_2^2} \\ a_{TE} &= \frac{n_2^2 - n_3^2}{n_1^2 - n_2^2} \end{aligned} \tag{5.29}$$

These definitions result in the dispersion curves depicted in figure 5.9 for TE eigenmodes (for different values of the asymmetry factor a_{TE}.

The number of guided TE modes can be calculated from equation 5.50 to 5.27:

$$M = 1 + \mathrm{Int}[\frac{1}{\pi}(\nu - \mathrm{Arctan}(\sqrt{a}_{TE})] \tag{5.30}$$

In this equation Int[...] means the integer part of the argument. For symmetrical waveguides this formula is simplified to $M = 1 + \mathrm{Int}[\frac{\nu}{\pi}]$. So there is at least 1 guided mode. In the case of a symmetrical waveguide knowing the normalized frequency ν is sufficient to determine the amount of guided modes. Therefore this number is frequently used when describing optical waveguides.

Note that the effective index can be considered as some kind of average refractive index felt by the guided mode. In this context we can also define the confinement factor Γ. It is defined (for TE polarization) as

$$\Gamma_i^{TE} = \frac{\int_i E_y^2 dx}{\int_{-\infty}^{+\infty} E_y^2 dx} \tag{5.31}$$

and is a measure for the confinement of the eigenmode inside layer i. Obviously

$$\sum_{i=1}^{N} \Gamma_i^{TE} = 1 \tag{5.32}$$

The confinement factor is often used in the theory of laser operation, to denote which part of the optical power is located inside the active layer, where there is gain.

5.2.4 The effective index method

Lets return to the two-dimensional waveguide. For many waveguide types the lateral dimensions are larger than the transversal dimensions. Moreover, the vertical index contrast often is very low. In that case, the modes of the waveguide often will show a quasi-TE or quasi-TM behaviour and can be approximately described by the scalar Helmholtz equation. The effective index method gives an approximate solution to this equation.

As said, the starting point for the effective index method is the scalar Helmholtz equation:

$$\nabla^2 \Psi(x,y,z) + k_0^2 n^2(x,y)\Psi(x,y,z) = 0 \tag{5.33}$$

In this equation Ψ can be replaced by any of the field components. Because we are still considering longitudinally invariant waveguide structures, the z dependence of $\Psi(x,y,z)$ is given by

$$\Psi(x,y,z) = \psi(x,y)e^{-j\beta z} \tag{5.34}$$

This way, equation (5.33) becomes

$$\nabla_{xy}^2 \psi(x,y) + (k_0^2 n^2(x,y) - \beta^2)\psi(x,y) = 0 \tag{5.35}$$

This equation can be solved in a number of ways. A first method is the effective index method which is an approximate solution. We start from the assumption that we can write

$$\psi(x,y) = F(x,y)G(y) \tag{5.36}$$

in which $F(x,y)$ is a slowly varying function of y, so that we can write that

$$\frac{\partial F}{\partial y} = 0 \tag{5.37}$$

Substitution of equation 5.36 in equation 5.35 leads to

$$F(x,y)\frac{d^2G(y)}{dy^2} + 2\frac{\partial F(x,y)}{\partial y}\frac{dG(y)}{dy} + G(y)\left[\frac{\partial^2 F(x,y)}{\partial x^2} + \frac{\partial^2 F(x,y)}{\partial y^2}\right] + (n^2k_0^2 - \beta^2)F(x,y)G(y) = 0 \tag{5.38}$$

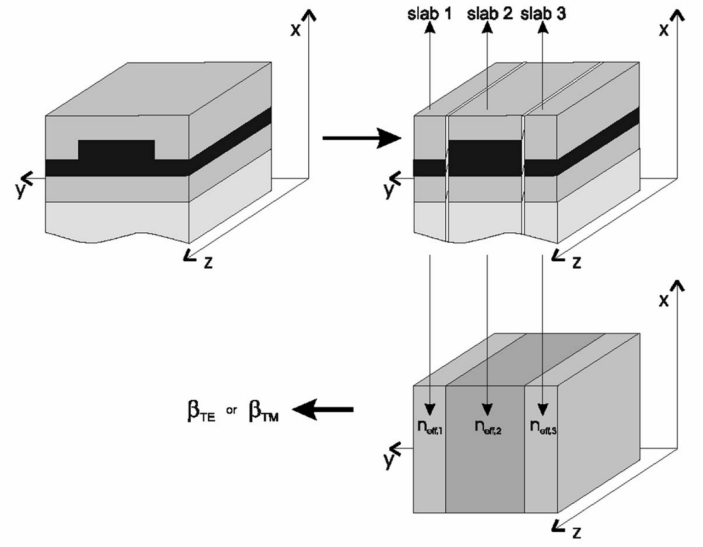

Figure 5.10: Effective index method

Using equation 5.37 this becomes

$$\frac{1}{G}\frac{d^2G}{dy^2} + \frac{1}{F}\frac{\partial^2 F}{\partial x^2} + (k_0^2 n^2(x,y) - \beta^2) = 0 \tag{5.39}$$

We now apply a technique closely resembling the classical technique of separation of variables. The only difference is that $F(x,y)$ shows a weak dependence on y and that we have to introduce an y-dependent separation variable $n_{eff}(y)$. This way we find

$$\begin{array}{l} \frac{1}{F}\frac{\partial^2 F}{\partial x^2} + k_0^2 n^2(x,y) = k_0^2 n_{eff}^2(y) \\ \frac{1}{G}\frac{d^2G}{dy^2} - \beta^2 = -k_0^2 n_{eff}^2(y) \end{array} \tag{5.40}$$

These are the fundamental equations of the effective index method. Lets consider the first equation. We divide the two dimensional waveguide in slices for which we can assume the refractive index profile as being independent of y. This is very easy for piecewise constant refractive index profiles but is also possible for a continuously varying index profile by applying a staircase approximation (figure 5.10).

Equation (5.40) then reduces to

$$\frac{\partial^2 F_i}{\partial x^2} + k_0^2 n_i^2(x) F_i = k_0^2 n_{eff,i}^2 F_i \tag{5.41}$$

If we compare this equation with equation (5.17a) then it is clear that $n_{eff,i}$ is the effective index of a one dimensional slab waveguide with a refractive index profile $n_i(x)$. The corresponding mode profile determines $F_i(x)$. Solving the first equation of (5.40) leads to an effective index distribution $n_{eff}(y)$. Using this function we can solve the second equation of (5.40). This equation can be rewritten as

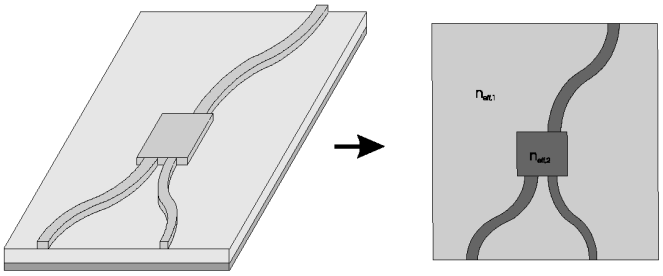

Figure 5.11: one dimensional equivalent

$$\frac{d^2G}{dy^2} + (k_0^2 n_{eff}^2(y) - \beta^2)G = 0 \tag{5.42}$$

Again, this is the equation for a one dimensional slab waveguide with refractive index profile $n_{eff}(y)$. Solving this equation results in the propagation constant β and the mode profile $G(y)$.

Although this method is in principle a scalar method, it still allows to take the polarization of the mode $\psi(x, y)$ into account. Say we are interested in the TE eigenmode of the two dimensional waveguide. The electric field vector of the mode is pointing along the y-axis, just like for the TE slab modes $F_i(x)$. To keep the same polarization state for the second equation this equation has to be solved for TM polarization. To calculate the TM eigenmode of the two dimensional waveguide, the appropriate boundary conditions need to be applied.

The errors made using the effective index method are due to the fact that equation (5.37) does not apply. This is the case in the vicinity of vertical dielectric interfaces. Generally speaking the effective index method will overestimate the propagation constants of the waveguide modes.

The effective index method is not only used to calculate two dimensional mode profiles and its corresponding propagation constants. More often it is used to simplify a two dimensional transversal waveguide structure to a one dimensional structure which can serve as a starting point for further analysis methods like the mode expansion method or the beam propagation method (figure 5.11).

5.2.5 Numerical methods

Numerical methods like finite difference or finite element methods start of from the vectorial equations or the scalar Helmholtz equation. In a finite difference method, the first step always is the discretization of the refractive index profile. To do this the waveguide is put inside a box with dimensions that are sufficiently large to suppose that the fields are zero on the edges of the box. Next, the box is divided into basic cells in which the refractive index is constant (meshing). Depending on the meshing algorithm, the mesh will or will not be equidistant.

In a second step the field equations are discretized by replacing the derivatives by their finite difference representation. In this way the set of partial differential equations is replaced by a linear set of equations which can be solved using standard algebraic methods.

The errors due to the finite difference method have two causes. There is the finite difference approximation of the derivatives and on the other side the approximation that the fields are zero

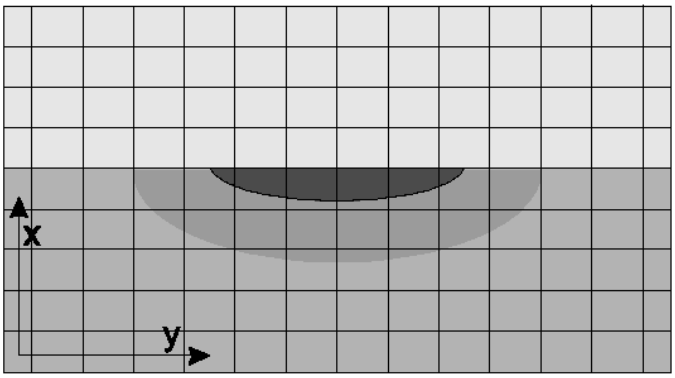

Figure 5.12: Discretization for numerical methods

on the edges of the box. To reduce these errors the discretization of the mesh can be refined and the dimensions of the box can be increased.

Note that there is a fundamental difference between the errors due to an approximate method like the effective index method and a numerical method like the finite difference method. With numerical methods we can start of with the exact Maxwell equations and the error can always be reduced by refining the discretization parameter, at the expense of larger calculation times. In approximated methods like the effective index methods, the equations are solved rigorously, but the equations are only approximations of Maxwells equations.

5.2.6 Modes of metal-dielectric surface plasmon waveguide structures

In this section we will discuss the waveguiding properties of an interface between a semi-infinite metal with a complex permittivity $\varepsilon_m = \varepsilon'_m + j\varepsilon''_m$ and a semi-infinite dielectric with permittivity $\varepsilon_d = \varepsilon'_d + j\varepsilon''_d$, as shown in figure 5.2.6.

While this layer structure consists only of two semi-infinite materials, one can still look for guided modes with a propagation constant β. If these guided modes exist, their propagation constants can be found by solving the eigenvalue equation 5.27 and 5.28 for TE and TM polarization respectively, by letting d approach to zero, as this two-layer waveguide can be treated as a limiting case of the three-layer waveguide stack discussed in the previous section. For TE polarization, this results in an eigenvalue equation

$$\gamma = -\delta \tag{5.43}$$

while for TM polarization the eigenvalue equation becomes

$$\frac{\gamma}{\varepsilon_m} + \frac{\delta}{\varepsilon_d} = 0 \tag{5.44}$$

with

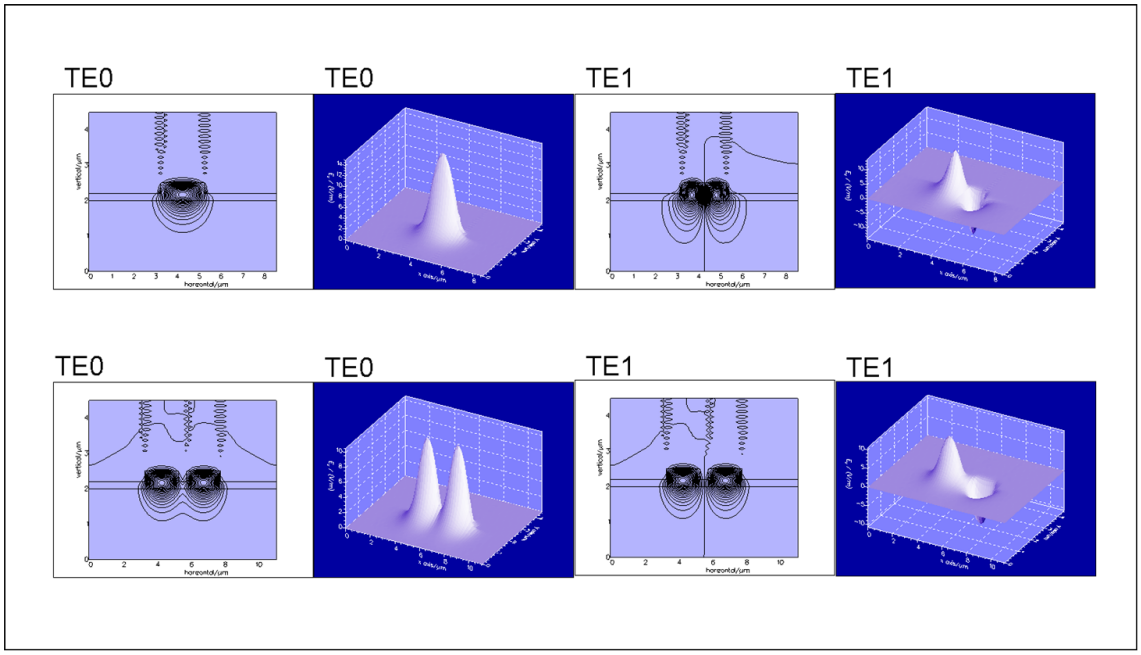

Figure 5.13: Example of 2D mode calculation using a numerical method. The upper row of plots shows the 0th and 1st order TE mode of a rib waveguide. The second row of plots shows the symmetric and antisymmetric TE mode in two coupled waveguides of the same type as the first row.

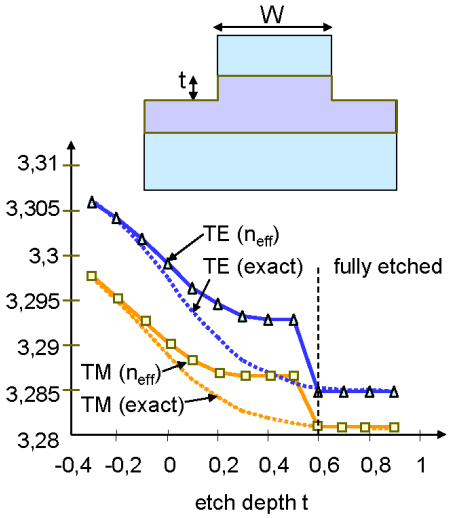

Figure 5.14: In this graph we show the effective index of the 0th order mode (TE and TM) of the depicted rib waveguide, calculated using a numerical mode solver (exact) and the effective index method. The guiding layer of the rib waveguide is 0.6μm thick. In the low index contrast case (not etched in the guided layer ($t < 0$)) the results of the effective index method closely resemble the exact results. Also when the waveguide is etched completely through the guiding layer ($t > 0.6\mu m$) this is the case. Only in the intermediate area the approximation is less good.

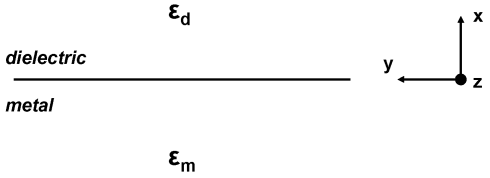

Figure 5.15: interface between a semi-infinite dielectric and a semi-infinite metal

$$\gamma = \sqrt{\beta^2 - \omega^2\mu_0\varepsilon_0\varepsilon_m} \text{ and } \delta = \sqrt{\beta^2 - \omega^2\mu_0\varepsilon_0\varepsilon_d} \tag{5.45}$$

The eigenvalue equation for TE polarization yields no solution: assume that there would be a solution β_{TE}, inserting this solution in 5.43 would result in the requirement that $\varepsilon_m = \varepsilon_d$ (and $\beta_{TE} = \omega\mu_0\varepsilon_0\varepsilon_d$), which represents the case of a plane wave solution in a uniform medium. For TM polarization, we can rewrite the eigenvalue equation as:

$$\beta = \frac{\omega}{c}\sqrt{\frac{\varepsilon_d\varepsilon_m}{\varepsilon_d + \varepsilon_m}} \tag{5.46}$$

For a lossless metal and dielectric ($\varepsilon''_m = \varepsilon''_d = 0$), we can write

$$\beta = \frac{\omega}{c}\sqrt{\frac{\varepsilon'_d\varepsilon'_m}{\varepsilon'_d + \varepsilon'_m}} \tag{5.47}$$

A guided mode exists if β is real (as an imaginary β would result in an exponentially decaying field without oscillations, which carries no power). There are two possibilities to satisfy this requirement (assuming a positive ϵ'_d):

$$\varepsilon'_m > 0 \tag{5.48}$$

or

$$\varepsilon'_m < 0 \text{ and } \left|\varepsilon'_m\right| > \varepsilon'_d \tag{5.49}$$

Substituting equation 5.47 in equation 5.45, one finds an expression for γ and δ, which describe the field profile of the electromagnetic mode as

$$\begin{cases} h_y = Ae^{-\delta x} & (x \geq 0) \\ h_y = Ae^{\gamma x} & (x \leq 0) \end{cases} \tag{5.50}$$

in analogy with the mode profile for TE polarized waveguide modes for dielectric waveguides in equation 5.50 (letting d go to zero and also taking into account the continuity of h_y at the interface).

In this equation, γ and δ are give by

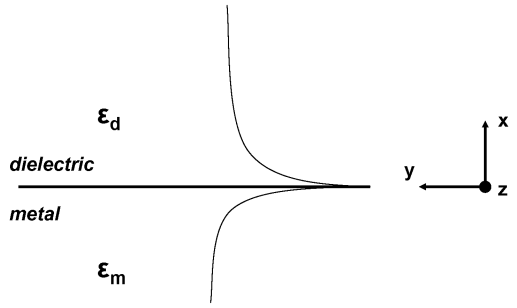

Figure 5.16: h_y-field of a surface plasmon propagating at the interface between a semi-infinite dielectric and a semi-infinite metal

$$\gamma = \frac{\omega}{c}\sqrt{\frac{-\varepsilon_m'^2}{\varepsilon_m' + \varepsilon_d'}} \tag{5.51}$$

and

$$\delta = \frac{\omega}{c}\sqrt{\frac{-\varepsilon_d'^2}{\varepsilon_m' + \varepsilon_d'}} \tag{5.52}$$

When $\varepsilon_m' < 0$ and $|\varepsilon_m'| > \varepsilon_d'$ (condition 5.49), both γ and δ are real and positive, implying that the h_y field component of the mode guided at the metal-dielectric interface consists of two exponentially decaying functions, as shown in figure 5.2.6. This mode, which exists at the interface between a semi-infinite dielectric and (perfect) metal is referred to as a surface plasmon mode. The e_x and e_z field components can easily be calculated from equation 5.16. These are also exponentially decaying (with e_z being continuous at the interface, while there is a discontinuity in the e_x component). The fields typically penetrate much deeper into the dielectric than into the metal. The fact that the field peaks at the interface, makes the propagation properties of the surface plasmon mode very sensitive to possible variations in the refractive index at the metal-dielectric interface and these modes can therefore be used to sense the presence of a very thin layer at the metal surface (e.g. the detection of a monolayer of proteins at a chemically activated gold surface).

When $\varepsilon_m' > 0$, γ and δ will be imaginary, meaning that the light will not be bound to the interface, and radiate into the two semi-infinite media (radiative surface plasmon mode).

While we assumed a perfect metal in the above discussion, the theory can be extended for the case of a lossy metal. The above conclusions remain valid, while the propagation constant obtains an imaginary part which describes the loss the surface plasmon mode experiences when travelling along the metal-dielectric interface. Propagation lengths are typically in the order of 10 to 100μm, depending on the metal used and the wavelength.

The real part of the dielectric function of a metal can be described by (according to the free electron model of Drude)

$$\varepsilon_1'(\omega) = 1 - \frac{\omega_p^2}{\omega^2} \tag{5.53}$$

with ω_p the plasma-frequency. Therefore, a non-radiating surface plasmon ($\varepsilon'_m < 0$ and $|\varepsilon'_m| > \varepsilon'_d$) can only exist when

$$\omega < \frac{\omega_p}{\sqrt{1+\varepsilon'_d}} \tag{5.54}$$

while radiating surface plasmons ($\varepsilon'_m > 0$) occur when $\omega > \omega_p$.

5.3 Propagation through dielectric waveguide structures

In this section we will discuss the propagation of light through waveguide structures for which the transversal cross section varies along the propagation direction. In some cases approximated semi-analytical calculation methods can be used (mode expansion, coupled mode theory, supermode theory). In most cases a complete numerical treatment will be necessary.

5.3.1 Mode expansion and propagation method

We assume a one dimensional z invariant waveguide that is excited by a field distribution $\Psi(x,z)$ and we want to see how this field looks like after propagating through the waveguide over a distance L.

The eigenmodes of the waveguide form a complete set and are orthonormal, so we can write

$$\Psi(x,z=0) = \sum_{i=0}^{N-1} a_i \psi_i(x) \quad \text{with} \int_{-\infty}^{+\infty} \psi_i(x)\psi_j(x)dx = \delta_{ij} \tag{5.55}$$

In this equation ψ_i is the i-th eigenmode of the waveguide. This sum includes all eigenmodes (both the guided and radiating eigenmodes, for which the sum actually has to be replaced by an integral). The expansion coefficients a_i can easily be calculated. By multiplying equation (5.55) with ψ_j and integrating this equation from $-\infty$ to $+\infty$ we find

$$a_j = \int_{-\infty}^{+\infty} \Psi(x,z=0)\psi_j(x)dx \tag{5.56}$$

The propagation of the individual eigenmodes through the waveguide is trivial (multiplying each eigenmode by its propagation factor $e^{-j\beta_j z}$). The field $\Psi(x,z)$after propagation through the waveguide over a distance L is then given by

$$\Psi(x,z=L) = \sum_{i=0}^{N-1} \left[\int_{-\infty}^{+\infty} \Psi(x,z=0)\psi_i(x)dx \right] \psi_i(x) e^{-j\beta_i L} \tag{5.57}$$

Suppose this waveguide is coupled to another, also z-invariant waveguide, with eigenmodes $\phi_i(x)$. If we assume that there are no reflections (which is an approximation), the output field of the first waveguide becomes the input field of the second waveguide. Just like in equation (5.55) we can decompose this field in the eigenmodes of the second waveguide

$$\Psi(x, z = L) = \sum_{i=0}^{N-1} a_i \psi_i(x) e^{-j\beta_i L} = \sum_{j=0}^{M-1} b_j \phi_j(x) \tag{5.58}$$

Because also the eigenfunctions $\phi_i(x)$ are orthonormal, we can find an expression for b_k:

$$b_k = \int_{-\infty}^{+\infty} \Psi(x, z = L)\phi_k(x)dx = \sum_{i=0}^{N-1} a_i \int_{-\infty}^{+\infty} \psi_i(x)\phi_k(x)dx e^{-j\beta_i L} \tag{5.59}$$

We can now propagate the field (5.58) through the second waveguide:

$$\Psi(x, z = L + L') = \sum_{j=0}^{M-1} b_j \phi_j e^{-j\gamma_j L'} \tag{5.60}$$

in which γ_j are the propagation constants of the eigenmodes in the second waveguide. This procedure can be repeated as often as required and can be written down easily in a matrix notation.

Note that at every vertical waveguide discontinuity a reflected field originates. So, not only the coupling of the eigenmodes of the first waveguide to the eigenmodes of the second waveguide needs to be taken into account, but also the coupling back to the eigenmodes of the first waveguide needs to be considered. When there is only a weak discontinuity these reflections can often be neglected and in such a case the unidirectional mode expansion propagation method described above applies. In some cases it is necessary however to include the reflections and then a bidirectional eigenmode expansion propagation method has to be used.

Figure 5.17a shows how the propagation of a field through a gradually broadening waveguide can be calculated by means of the mode expansion method. Here, the discontinuities are small and we can neglect the reflected field. For the codirectional coupler of figure 5.17b this is not the case. In this case reflections play an important role and a bidirectional method has to be used.

5.3.2 Coupled mode theory

In a regular z-independent waveguide, eigenmodes are orthonormal and propagate in an independent way. The complete field can be written as a linear combination of the eigenmodes. In some situations the waveguide structure can be seen as a small perturbation of the simple z-independent waveguide structure. In that case, the field can still be written in terms of the modes of the simple waveguide structure, but due to the perturbation these modes will no longer be decoupled. In the case two modes are dominant, the field can be written as:

$$\Psi(x, z) = C_1(z)e^{-j\beta_1 z}\psi_1(x) + C_2(z)e^{-j\beta_2 z}\psi_2(x) \tag{5.61}$$

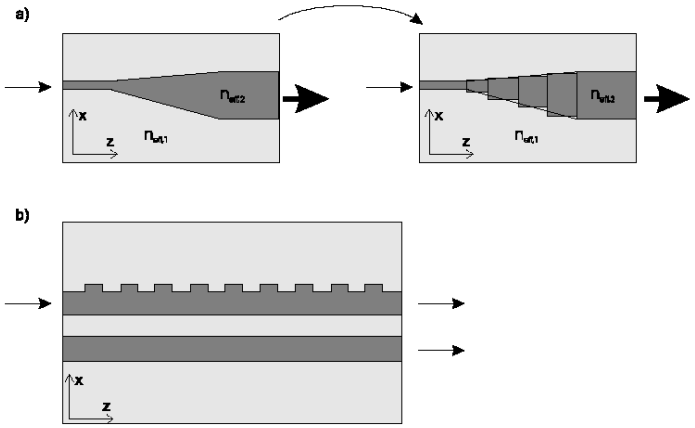

Figure 5.17: Waveguide structures

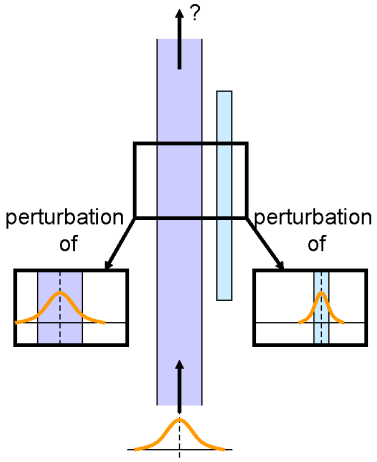

Figure 5.18: Coupled mode theory

Fast longitudinal variations are taken into account by the propagation factor $e^{-j\beta_i z}$ while the z-dependent coefficients $C_1(z)$ and $C_2(z)$ describe the coupling between the two modes ψ_1 and ψ_2. An alternative formulation takes all longitudinal variations together in one term $X_i(z)$:

$$\Psi(x,z) = X_1(z)\psi_1(x) + X_2(z)\psi_2(x) \tag{5.62}$$

We will continue to use the formulation used in equation (5.62). Depending on the envisioned structure an appropriate choice of ψ_1 and ψ_2 has to be made. In figure 5.18 a typical example is shown of a waveguide structure where coupled mode theory can be applied. Is this case we choose ψ_1 and ψ_2 to be the waveguide modes of the unperturbed waveguides. Note that we can consider this system to be double perturbed.

The uncoupled modes ψ_1 and ψ_2 satisfy following propagation equations:

$$\begin{array}{l} \frac{dX_1}{dz} = -j\beta_1 X_1 \\ \frac{dX_2}{dz} = -j\beta_2 X_2 \end{array} \tag{5.63}$$

with the obvious solution

$$\begin{array}{l} X_1(z) = e^{-j\beta_1 z} \\ X_2(z) = e^{-j\beta_2 z} \end{array} \tag{5.64}$$

Coupled mode theory postulates that linear coupling terms need to be added to this equation to describe the perturbed system

$$\begin{array}{l} \frac{dX_1(z)}{dz} = -j\beta_1 X_1(z) - j(\kappa_{11} X_1 + \kappa_{12} X_2) \\ \frac{dX_2(z)}{dz} = -j\beta_2 X_2(z) - j(\kappa_{21} X_1 + \kappa_{22} X_2) \end{array} \tag{5.65}$$

We will assume that the coupling coefficients are z-independent and that both modes travel in the same direction (uniform codirectional coupling). Normally, some other assumptions are also made:

- The two modes are normalized
- The total power flux in the system can be calculated by the sum of the power carried by every mode seperately:

  $$P(z) = |X_1|^2 + |X_2|^2 \tag{5.66}$$

  Modes have to be power independent for this.
- The complete system is lossless ($\frac{dP(z)}{dz} = 0$). If we calculate $\frac{dP(z)}{dz}$ by means of equation (5.66) and (5.65) we find that

  $$\begin{cases} \beta_1, \beta_2, \kappa_{11}, \kappa_{22} \text{ are real} \\ \kappa_{21} = \kappa_{12}* \end{cases} \tag{5.67}$$

- Based on reciprocity and symmetry around a plane parallel to z=0 we also find (both for lossless and lossy systems) that

  $$\kappa_{21} = \kappa_{12} \tag{5.68}$$

  This means that in the lossless case all coupling constants are real.

If we choose initial conditions to be $X_1 = 1$ and $X_2 = 0$, which means that only one of the modes is excited, integrating equation (5.65) leads to

$$\begin{array}{l} X_1(z) = e^{-j\beta z}\left[\cos(\delta z) - i\frac{\Delta}{\delta}\sin(\delta z)\right] \\ X_2(z) = e^{-j\beta z}\left[-i\frac{\kappa_{21}}{\delta}\sin(\delta z)\right] \end{array} \tag{5.69}$$

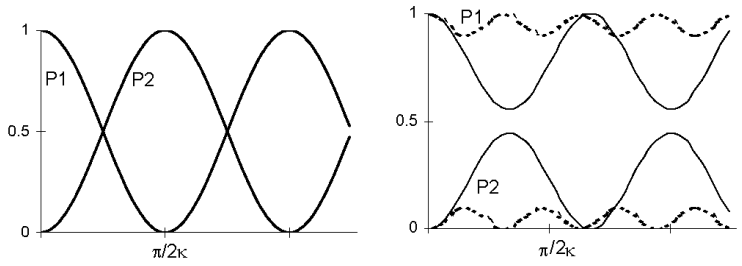

Figure 5.19: Variation of the power in the two modes ψ_1 and ψ_2. In the left graph $\Delta = 0$ (no phase mismatch). In the right graph the power exchange in the case of $\Delta = 1.113\kappa$ and $\Delta = 3.0\kappa$ (dashed line) is shown.

with

$$\begin{aligned} \beta &= (\beta_1 + \beta_2 + \kappa_{11} + \kappa_{22})/2 \\ \kappa &= \sqrt{\kappa_{12}\kappa_{21}} \\ \Delta &= (\beta_1 - \beta_2 + \kappa_{11} - \kappa_{22})/2 \\ \delta &= \sqrt{\Delta^2 + \kappa^2} \end{aligned} \tag{5.70}$$

with β the average propagation constant of both modes and Δ expressing the phase matching per length unit between both modes (note that in most cases κ_{11} and κ_{22} are small compared to β_1 and β_2, so $\Delta \approx \frac{\beta_1 - \beta_2}{2}$).

In figure 5.19 some typical variations of the power $P_1 = |X_1|^2$ and $P_2 = |X_2|^2$ are plotted as a function of z in the lossless case ($\kappa = \kappa_{12} = \kappa_{21}$). We can clearly see the periodic power exchange between the modes, for which the period and the amount of power exchanged depend on the coupling coefficient κ and the phase mismatch Δ.

- When there is no phase mismatch ($\Delta = 0$) complete power exchange occurs. This is the case when both modes have the same propagation constant. This case is also called synchronous coupling. The coupling length is

$$L_c = \frac{\pi}{2\kappa} \tag{5.71}$$

- As long as Δ remains smaller than κ, still an important power exchange occurs. With increasing phase mismatch, both the power exchange level and power exchange period decrease. The maximum power that can be coupled from one mode to another is given by

$$\frac{\kappa^2}{\kappa^2 + \Delta^2} \tag{5.72}$$

- For a large phase mismatch ($\Delta >> \kappa$) power exchange is negligible. The modes are no longer coupled.

We will now consider two typical examples in which the coupled mode theory can be applied.

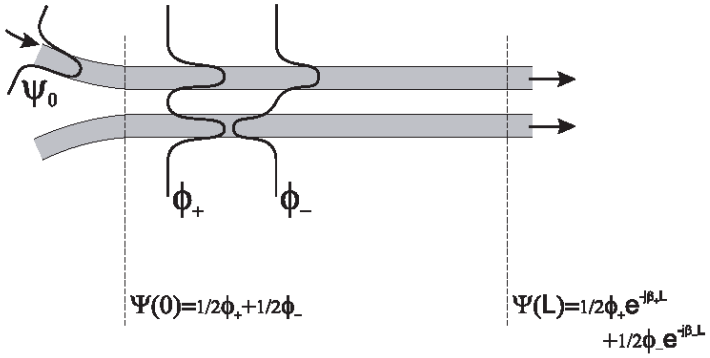

Figure 5.20: Directional coupler structure

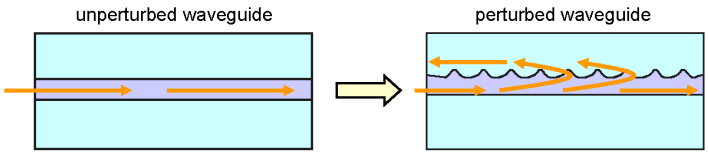

Figure 5.21: Contradirectional grating coupler

- Directional coupler

  In the case of a directional coupler, consisting of two waveguides running parallel to each other, the coupling coefficients can easily be calculated using perturbation theory (see Appendix). We find that

$$\begin{aligned} \kappa_{12} &= \frac{k_0^2}{2} \int (n_{12}^2 - {n_1}^2)\psi_1\psi_2 dx \\ \kappa_{21} &= \frac{k_0^2}{2} \int (n_{12}^2 - {n_2}^2)\psi_1\psi_2 dx \end{aligned} \tag{5.73}$$

- Contradirectional grating coupler

  In the case of a contradirectional grating coupler one chooses the modes ψ_1 and ψ_2 to be identical but propagating in the opposite direction. The theory described above can then be repeated, however we have to change equation (5.66) for the z-dependent power flux to

$$P(z) = |X_1|^2 - |X_2|^2 \tag{5.74}$$

  In the chapter on periodic structures this theory will be elaborated. Applications of the contradirectional coupler are DBR and DFB lasers.

5.3.3 Supermodes

An alternative calculation method uses the theory of supermodes [1]. Lets consider again a directional coupler consisting of two identical monomodal waveguides, both with fundamental mode

[1] Actually this is a simplified form of the general mode expansion theory described in 5.3.1

ψ_0. We can also look at the structure as a whole as being a single waveguide. In this waveguide structure a symmetrical and antisymmetrical mode ϕ_+ and ϕ_- with propagation constants β_+ and β_- can propagate (see also figure 5.13).

When we excite one of the waveguides with its modal field ψ_0 then we can write

$$\Psi(x, z = 0) = \psi_0(x) \approx c_+\phi_+ + c_-\phi_- \tag{5.75}$$

with $c_+ = c_- = 1/2$. After propagation over a distance L this becomes

$$\Psi(x, z = L) = c_+\phi_+ e^{-j\beta_+ L} + c_-\phi_- e^{-j\beta_- L} \tag{5.76}$$

or

$$\Psi(x, z = L) = c_+ e^{-j\beta_+ L}\left[\phi_+ + \phi_- e^{+j(\beta_+ - \beta_-)L}\right] \tag{5.77}$$

When $e^{+j(\beta_+ - \beta_-)L} = -1$ all power will be concentrated in the second waveguide. This way we find the following relation between the coupling coefficient κ and the difference $\beta_+ - \beta_-$:

$$\beta_+ - \beta_- = 2\kappa \tag{5.78}$$

Lets now consider an asymmetrical directional coupler. The modes will no longer be perfectly symmetrical and asymmetrical but tend to look like the modes of the individual waveguides. Equation (5.75) is still valid, but c_+ will no longer equal c_-.

After propagation over a distance L, we find

$$\Psi(x, z = L) = c_+ e^{-j\beta_+ L}\left[\phi_+ + \frac{c_-}{c_+}\phi_- e^{+j(\beta_+ - \beta_-)L}\right] \tag{5.79}$$

The period of power exchange still is given by

$$L_c = \frac{\pi}{\beta_+ - \beta_-} \tag{5.80}$$

but the power exchange is no longer complete. The amount of power exchange is given by $\frac{c_-}{c_+}$. So we can write

$$(\beta_+ - \beta_-) = 2\delta = 2\sqrt{\Delta^2 + \kappa^2} \tag{5.81}$$

and if $|\Delta| >> \kappa$

$$(\beta_+ - \beta_-) \approx 2\,|\Delta| \approx |\beta_1 - \beta_2| \tag{5.82}$$

In certain cases it occurs that the dispersion curves $\beta_1(\omega)$ and $\beta_2(\omega)$ of the uncoupled waveguides intersect at a certain frequency. This means that the directional coupler operates in phase matched

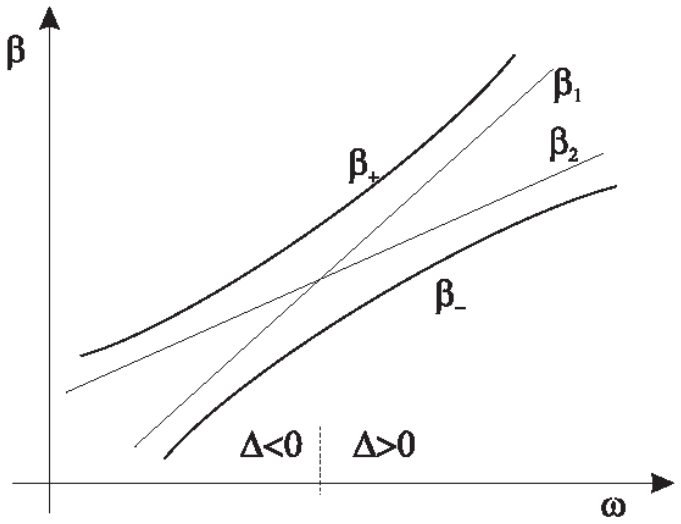

Figure 5.22: Dispersion curves of uncoupled modes and super modes

conditions for this frequency (so there is strong coupling) and for other frequencies the coupling is weak (asynchronous coupling). So we get the picture as shown in figure 5.22 in which $\beta_1, \beta_2, \beta_+$ and β_- are shown as a function of frequency. From this picture it is clear that at low frequency the supermodes resemble the propagation constant (and field profile) of one of the unperturbed modes. At the phase matching frequency this behaviour is broken and $\beta_+ - \beta_- = 2\kappa$. At higher frequencies this behaviour changes and each of the supermodes will resemble the other unperturbed waveguide mode.

5.3.4 Beam propagation method

1. Introduction

   The methods described in the previous sections only are applicable for a number of simple waveguide structures. In most cases there will be some coupling between guided and radiating modes. Because of this coupling, part of the optical power will be lost. The most important technique that takes into account this radiation loss is the beam propagation method (BPM). BPM allows to calculate the propagation of the optical field over a large distance (compared to the wavelength) and this for very complex structures. The required computer code is fairly simple and can easily be extended to waveguides with gain and loss, to waveguides with discrete longitudinal reflections or for polarization sensitive waveguide configurations like in the anisotropic $LiNbO_3$ crystal.

   The BPM-method can be used to model three dimensional waveguide structures. The simulation can be done in two ways. One can use a full three dimensional version of the BPM code. This leads to the most accurate results but is very time consuming. A less time consuming method is the combination of the effective index method and a two dimensional BPM. This eliminates the large index contrast with air and reduces the simulation time substantially. It is only useful however if the radiation towards the upper and lower half space

is negligible. In real structures this is often the case. Therefore, we will restrict ourself to the two dimensional BPM method. First we will discuss the classical FFT-BPM method.

2. FFT-BPM

Starting point of the discussion is the Helmholtz scalar wave equation in two dimensions

$$\nabla^2\Psi(x,z) + k_0^2 n^2(x,z)\Psi(x,z) = 0 \tag{5.83}$$

The square of the refractive index profile can be written as

$$n^2(x,z) = n_0^2 + \Delta n^2(x,z) \tag{5.84}$$

in which n_0 is a well chosen constant refractive index such that

$$\Delta n << n_0 \tag{5.85}$$

We propose a solution to equation (5.83) of the form:

$$\Psi(x,z) = \psi(x,z)e^{-jk_0n_0z} \tag{5.86}$$

The fast z-variations in $\Psi(x,z)$ are covered by the propagation factor $e^{-jk_0n_0z}$. We can assume that $\psi(x,z)$ will only be weakly z-dependent, such that

$$\left|\frac{\partial^2\psi}{\partial z^2}\right| << \left|2k_0n_0\frac{\partial\psi}{\partial z}\right| \tag{5.87}$$

This means that the amplitude function $\psi(x,z)$ varies slowly on the scale of the material wavelength $\frac{2\pi}{k_0n_0}$ (the so called paraxial approximation).

Substituting equation (5.86) into equation (5.83) we find that (taking equation (5.87) into account)

$$\frac{\partial\psi(x,z)}{\partial z} = -\frac{j}{2k_0n_0}\left(\frac{\partial^2\psi(x,z)}{\partial x^2} + k_0^2\Delta n^2(x,z)\psi(x,z)\right) \tag{5.88}$$

This is the scalar Fresnel equation or parabolic wave equation. We can write down equation (5.88) like

$$\frac{\partial\psi(x,z)}{\partial z} = (\hat{T}+\hat{N})\psi(x,z) \tag{5.89}$$

in which

$$\begin{array}{l}\hat{T} = -\frac{j}{2k_0n_0}\frac{\partial^2}{\partial x^2} \\ \hat{N} = \frac{-jk_0}{2n_0}\Delta n^2\end{array} \tag{5.90}$$

Integration of equation (5.88) can formally be determined to be

$$\psi(x, z + \Delta z) = e^{(\hat{T}+\hat{N})\Delta z}\psi(x, z) = e^{\hat{T}\Delta z}\left[e^{\hat{N}\Delta z}\psi(x, z)\right] \tag{5.91}$$

In this solution the step Δz has to be chosen sufficiently small. On the one hand because then $\Delta n(x, z)$ can be assumed z-independent over this step, on the other hand because stating that

$$e^{(\hat{T}+\hat{N})\Delta z}\psi(x, z) = e^{\hat{T}\Delta z}\left[e^{\hat{N}\Delta z}\psi(x, z)\right] \tag{5.92}$$

which means that we apply the operators $\hat{T}$ and $\hat{N}$ sequentially and not together, is only valid for sufficiently small Δz.

This way the field is propagated stepwise through the complete waveguide structure. We will now study the operator $e^{(\hat{T}+\hat{N})\Delta z}$. Calculating the term $\left[e^{\hat{N}\Delta z}\psi(x, z)\right]$ is straightforward. The field $\psi(x, z)$ is multiplied by an x-dependent phase term. The meaning of the operator $e^{\hat{T}\Delta z}$ is less obvious. Therefore we will first study the influence of the operator on a plane wave $\psi = e^{-jk_x x}$. Developing the operator in a Taylor expansion, we can write:

$$\begin{aligned} e^{\hat{T}\Delta z}e^{-jk_x x} &= e^{-\frac{j\Delta z}{2k_0 n_0}\frac{\partial^2}{\partial x^2}}e^{-jk_x x} \\ &= \left(1 + (-\tfrac{j\Delta z}{2k_0 n_0}\tfrac{\partial^2}{\partial x^2}) + \tfrac{1}{2}(-\tfrac{j\Delta z}{2k_0 n_0}\tfrac{\partial^2}{\partial x^2})^2 + ...\right)e^{-jk_x x} \\ &= (1 + \tfrac{j}{2k_0 n_0}\Delta z k_x^2 + \tfrac{1}{2}\left(\tfrac{j}{2k_0 n_0}\Delta z k_x^2\right)^2 + ...)e^{-jk_x x} \\ &= e^{\frac{j}{2k_0 n_0}\Delta z k_x^2}e^{-jk_x x} \end{aligned} \tag{5.93}$$

Therefore the influence of the operator on a plane wave can easily be calculated. Therefore, to calculate the influence of the operator on an arbitrary field $\psi(x, z)$ we first take the fourier transform of the field. On this plane wave expansion we can apply the operator $e^{\hat{T}\Delta z}$. By doing an inverse fourier transform we find the result of $e^{\hat{T}\Delta z}\psi(x, z)$. Note that this is equivalent to the propagation of an arbitrary field through a homogenous medium with refractive index n_0.

The calculation of the propagated field $\psi(x, z = \Delta z)$ out of the original field $\psi(x, z)$ is done as follows. First a phase correction, due to the index perturbation, is applied (operator $e^{\hat{N}\Delta z}$). Then the field is decomposed into its plane wave components, these are individually propagated through a homogenous medium with refractive index n_0 and then recomposed to the complete field distribution (operator $e^{\hat{T}\Delta z}$).

Note: Calculating $e^{(\hat{T}+\hat{N})\Delta z}\psi(x, z)$ as $e^{\hat{T}\Delta z}\left[e^{\hat{N}\Delta z}\psi(x, z)\right]$ is only an approximation. This is because the operators do not commute. A better approximation is to write

$$e^{(\hat{T}+\hat{N})\Delta z}\psi(x, z) = e^{(\frac{\hat{T}}{2})\Delta z}e^{\hat{N}\Delta z}e^{(\frac{\hat{T}}{2})\Delta z}\psi(x, z) + O(\hat{T}^3, \hat{N}^3) \tag{5.94}$$

The analysis is completely analogous to the previous one.

3. Expanding the theory

   FFT-BPM method is not often used any more. In most commercial modeling tools a finite difference BPM algorithm is used. In a finite difference BPM the paraxial wave equation is directly discretized, both longitudinally and transversally. Other extensions to the BPM algorithm are related to

- the waveguide structure which is not paraxial (i.e. equation (5.87) is no longer valid)
- vectorial calculations
- reflections
- 3D waveguides
- numerical accuracy and efficiency
- high contrast waveguides
- improved boundary conditions

5.4 Optical components

5.4.1 Loss in straight waveguides

In the previous section the straight waveguide was already extensively analyzed. In this section we will therefore restrict ourself to an aspect that has not yet been dealt with: propagation losses in waveguides. There are different causes for this loss. The interaction of light and matter result in absorption and non perfect guiding results in scattering and radiation losses.

When the origin of the loss is uniformly spread over the waveguide length, the guided optical power will decrease exponentially with the propagation distance.

$$P(z) = P_0 e^{-\alpha z} \tag{5.95}$$

α is called the power attenuation coefficient. Due to the typical dimensions of an integrated optical circuit (cm scale) α typically has to be below 0.1 to 1.0 cm^{-1}, which corresponds to a loss between 0.5dB/cm to 5dB/cm. We will now discuss the different loss mechanisms which cause these losses.

- Loss through absorption

  In semiconductor materials with a direct bandgap, the easiest absorption mechanism is the electron-hole pair creation by a photon with a photon energy larger than the bandgap E_g. Sometimes this is wanted (photodetectors) and if this is not the case it can easily be prevented by choosing a material composition with a bandgap sufficiently large compared to the photon energy.

  Also free carriers play a role in the absorption process due to inter and intraband transitions. For non-intentionally doped semiconductors with a carrier concentration of about $10^{16} cm^{-3}$ this absorption typically remains below 0.1dB/cm. Also in non semiconductor material losses occur due to electronic and molecular transitions.

- Loss through scattering

  Scattering losses are caused by spatial fluctuations of the refractive index (volume scattering) or by the roughness at the sidewalls of the waveguide (surface roughness scattering). These can be both etched waveguide boundaries that determine the waveguide or the interface of two layers which are grown on top of each other. In practice mostly surface roughness scattering seems to be a problem. Based on some simple assumptions, following approximated equation for the scattering loss at boundaries can be obtained

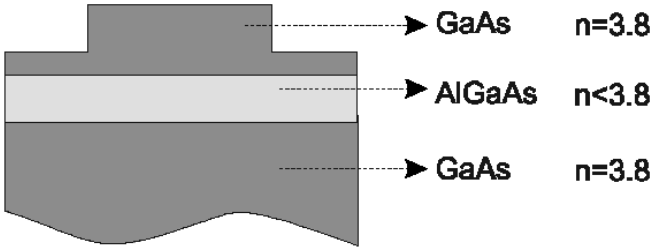

Figure 5.23: GaAs waveguide structure with radiation to the substrate

$$\alpha = \alpha_{scat} \frac{(\Delta n)^2 E_s^2}{P} \tag{5.96}$$

Δn is the index contrast at the interface, P is the power in the optical field and E_s is the field strength at the edges of the waveguide. The constant α_{scat} can only be empirically determined and depends on the etching process used.

One type of waveguides where special care has to be taken to limit the scattering loss are the deeply etched waveguides because the refractive index contrast between air and semiconductor is very high.

- Loss through radiation

  Loss through radiation is due to the non perfect guiding of the waveguide. The simplest example is a waveguide core that is not positioned between two layers with a lower refractive index. In that case there will be no total internal reflection and power will leak out of the waveguide.

  Another possibility is the case in which the waveguide core is positioned in between two layers with lower refractive index, but where there is however an area with higher refractive index nearby, to which optical power can leak. This process is comparable to the quantum mechanical tunneling of charged particles through a potential barrier. This situation frequently occurs in GaAs/AlGaAs waveguides existing of a GaAs waveguide core cladded by AlGaAs material and grown on a GaAs substrate. The AlGaAs material compositions that can be grown lattice matched on a GaAs substrate have a refractive index lower than that of GaAs, so power will leak from the waveguide core to the substrate. An example of such a waveguide is shown in figure 5.23. By increasing the thickness of the AlGaAs cladding layer, radiation losses can be limited.

5.4.2 Bent waveguides

Bent waveguides show a fundamental radiation loss. In straight waveguides the tendency for light to diffract is compensated by the higher refractive index of the waveguide core and the waveguide mode has flat phase fronts. In bent waveguides the phase front is rotating around a rotation center. Because the group velocity of the phase fronts can not exceed the local speed of light (c/n), there is a point where the phase front bends and where radiation occurs (figure 5.24).

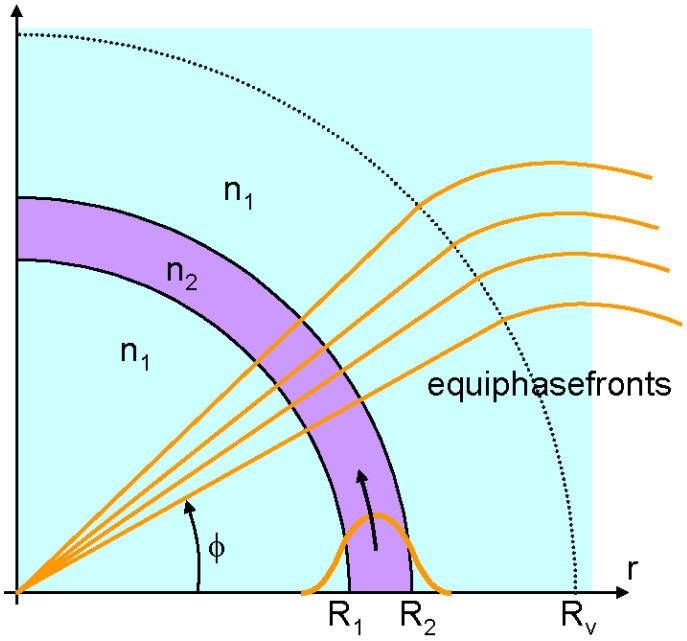

Figure 5.24: Bent waveguide

Bent waveguides place designers in a dilemma: radiation losses increase nearly exponentially with decreasing bend radius. The integration of multiple components on a semiconductor wafer (InP: maximum 2 inch wafers , Silicon: typically 8 inch wafers) requires waveguides that can change propagation direction on a short distance and without too many losses.

For the theoretical treatment we start off again from a two dimensional waveguide, possibly obtained by applying the effective index method. To calculate the waveguide modes we change to a cylindrical coordinate system r, ϕ. The edges of the bent waveguide will coincide with the coordinate planes $r = R_1$ and $r = R_2$. In this coordinate system the Helmholtz equation can be written as

$$\left(\frac{\partial^2}{\partial r^2} + \frac{1}{r}\frac{\partial}{\partial r} + \frac{1}{r^2}\frac{\partial^2}{\partial \varphi^2} + k_0^2 n^2(r)\right)\Psi(r,\varphi) = 0 \tag{5.97}$$

with $n(r)$ the refractive index profile. We propose a solution

$$\Psi(r,\varphi) = \psi(r)\Phi(\varphi) \tag{5.98}$$

$\psi(r)$ describes the bend mode profile, while $\Phi(\phi)$ determines the propagation. Substituting this equation in the Helmholtz equation results in

$$\left(\frac{r^2}{\psi(r)}\frac{\partial^2}{\partial r^2} + \frac{r}{\psi(r)}\frac{\partial}{\partial r} + \frac{r^2}{\psi(r)}k_0^2 n^2(r)\right)\psi(r) = -\frac{1}{\Phi(\varphi)}\frac{\partial^2\Phi(\varphi)}{\partial\varphi^2} \tag{5.99}$$

While the left side of equation (5.99) only depends on r and the right side only depends on ϕ we can equate both sides with a constant β_ϕ^2. Therefore we can write

$$\frac{1}{\Phi(\varphi)}\frac{\partial^2\Phi(\varphi)}{\partial\varphi^2} + \beta_\phi^2 = 0 \tag{5.100}$$

The general solution to this equation is

$$\Phi(\varphi) = Ce^{\pm j\beta_\phi\phi} \tag{5.101}$$

The solution is analogous to the solution for propagation in a straight waveguide. The phase fronts coincide with $\phi = cte$ planes. So they turn around the bend. β_ϕ is called the angular propagation constant (dimension rad^{-1}).

The left side of equation (5.99) can be solved directly by using Bessel functions. This requires the calculation of Bessel functions with large and complex indices, which leads to a lot of numerical problems. Another way of solving this equation is the so called conformal transformation. By substituting $r = R_t e^{\frac{u}{R_t}}$ we can write equation (5.99) like

$$\left[\frac{\partial^2}{\partial u^2} + (k_0^2 n_t^2(u) - \beta_t^2)\right]\psi(u) = 0 \tag{5.102}$$

in which $n_t(u) = n(u)e^{\frac{u}{R_t}}$ and $\beta_t = \frac{\beta_\phi}{R_t}$.

This means that in the (u, ϕ) coordinate system the Helmholtz equation has exactly the same shape as in a cartesian coordinate system (x, z) when we replace the refractive index profile $n(u)$ by the transformed index profile $n_t(u)$. Modes and propagation constants in bent waveguides can therefore be calculated by a mode solver developed for solving straight waveguide modes, by introducing the transformed index profile $n_t(u)$. This is schematically depicted in figure 5.25.

Figure 5.26 gives an example of a refractive index profile and the corresponding bend mode profile for different values of the radius of curvature. Based on the transformed refractive index profile it is easy to understand what happens in a bend:

- From the point where

  $$\mathrm{Re}(\beta_t) = n_t(u)k_0 \tag{5.103}$$

  radiation will occur and the phase front will bend backwards. That way propagation losses occur.

- The mode is most strongly guided in the area with the highest refractive index. Therefore, the mode profile will shift towards the outer rim of the bent waveguide. At the transition from straight to bent waveguide mode adaptation losses will occur.

- By decreasing the ring radius, the mode will completely move towards the outer edge of the waveguide so that the inner edge of the waveguide does not longer contribute to the guiding of the mode. These modes are called whispering gallery modes. The width of the waveguide is no longer an issue in the whispering gallery regime.

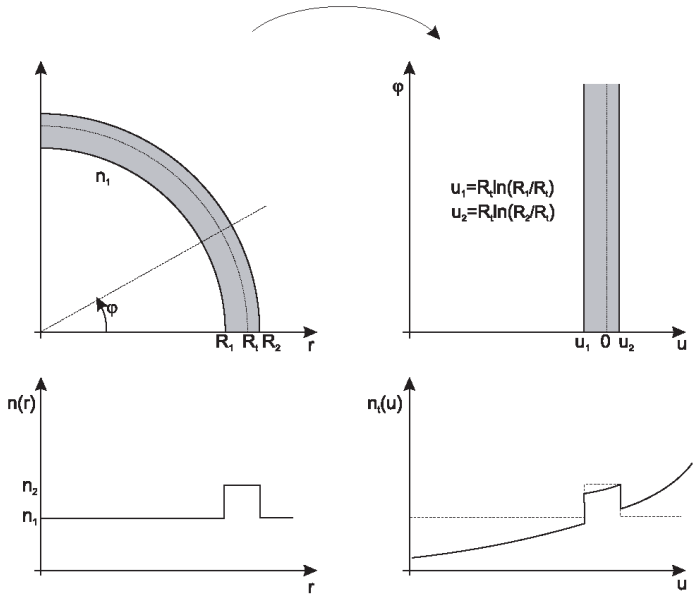

Figure 5.25: Conformal transformation

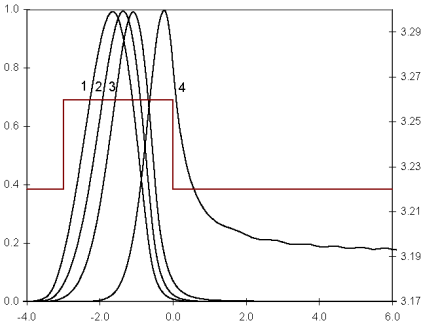

	R(μm)	α(dB/90)	offset(μm)
1	1000	0	0.38
2	500	0.01	0.63
3	300	0.19	0.85
4	100	18.35	1.25

Figure 5.26: Bend mode profiles

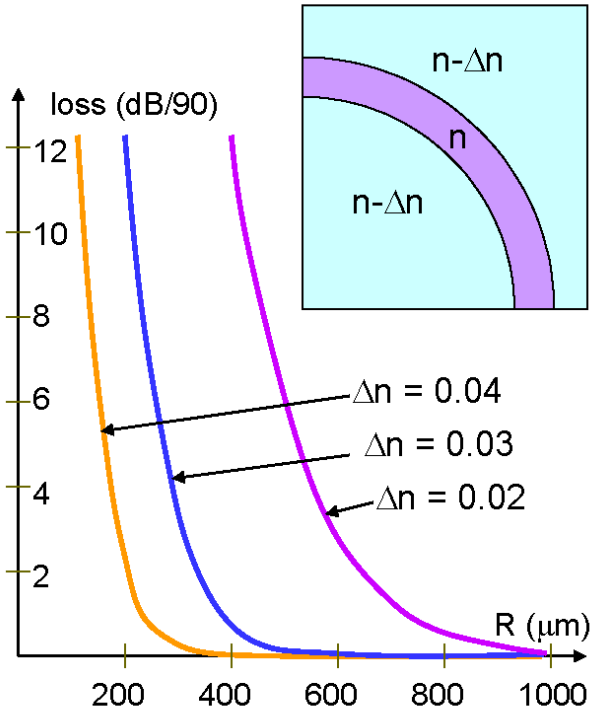

Figure 5.27: Bend mode loss (dB/90 degrees) as a function of radius and refractive index contrast

- By the increased field strength at the outer edge of the waveguide scattering losses will also increase.

These effects are all clearly visible in figure 5.26.

- Radiation losses

  Because the refractive index will be larger than the effective index of the waveguide mode at a certain distance from the bend, the effective index of a waveguide bend mode will be complex. We can write the angular propagation constant as

$$\beta_\phi = \beta'_\phi + j\alpha_\phi \tag{5.104}$$

  and

$$\alpha_\phi = \alpha_t R_t = -\mathrm{Im}(n_{eff,t}) k_0 R_t \tag{5.105}$$

  Figure 5.27 shows the attenuation coefficient as a function of the radius and the refractive index contrast as a parameter. It is clear that the loss increases rapidly below a certain critical bend radius.

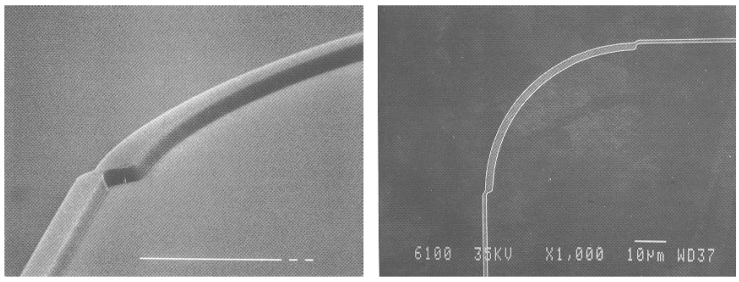

Figure 5.28: Adaptations at a straight waveguide / bend waveguide interface

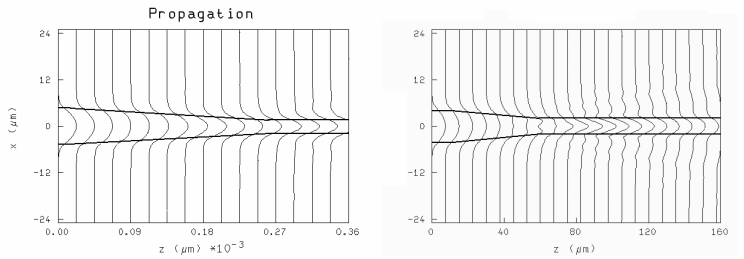

Figure 5.29: BPM calculation of an adiabatic (250um long) and a non-adiabatic (50um long) taper. Both tapers have a straight input waveguide of 10um long and a straight output waveguide of 100um.

- Mode adaptation losses

  In the bend, the mode profile is shifted outwards and is narrower than in the straight waveguide. The adaptation losses between straight and bent waveguide can be reduced by reducing the width of the straight waveguide and giving this waveguide an offset with respect to the bend, such that both waveguide profiles correspond better. The adaptation losses can be calculated by calculating the overlap integral of the bend mode and the mode in the straight waveguide. An adapted straight waveguide / bend interface is shown in figure 5.28.

5.4.3 Tapers

1. General description

   A taper is a smooth transition between two waveguides of different widths or height and is used to couple two components with different waveguide geometry. Changes in the waveguide structure result in mode conversion. This means that power is exchanged between the different modes of the waveguide. When power is coupled to radiating modes, loss occurs, but also in the case of multimodal waveguides it is often unwanted that the power is distributed over different waveguide modes. Mode conversion can be suppressed when the change in waveguide structure is very gentle. In the case we call the adaptation of the mode profile adiabatic. An adiabatic transition between two waveguide structures is a transition where the mode of the system adapts to the changing geometry without loosing power by conversion to other modes. To analyze taper structures numerical methods need to be used: BPM method or mode expansion and propagation method applied to a staircase approximation of the taper profile.

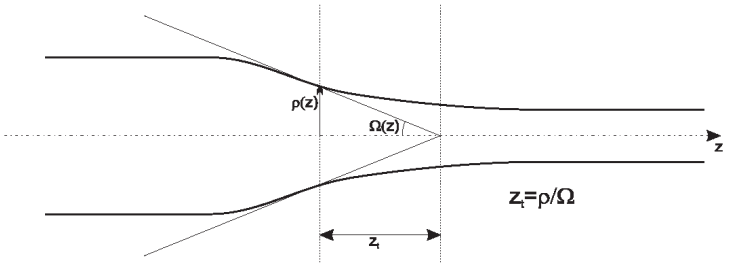

Figure 5.30: Definition of the local taper length

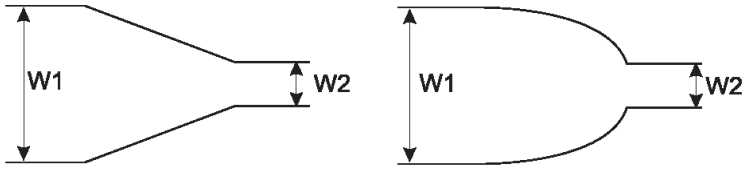

Figure 5.31: The linear and parabolic taper

Based on some intuitive considerations it still is possible to derive a criterion to calculate the maximum adiabatic taper angle, which allows an adiabatic transition. As said before, the fundamental mode will transform adiabatically when no power coupling to higher order modes occurs. We can assume that especially the coupling to the second order mode is dominant (the first order mode is antisymmetrical). Based on this assumption, we propose the following criterion for adiabatic transitions: the taper will behave adiabatically when the local taper length is larger than the local coupling length between the fundamental mode and the next symmetrical mode. The local taper length z_t is defined as in figure 5.30.

$$z_t = \frac{\rho(z)}{\tan(\Omega(z))} \approx \frac{\rho(z)}{\Omega(z)} \tag{5.106}$$

The coupling length is given by

$$z_b = \frac{\pi}{\beta_0 - \beta_2} \tag{5.107}$$

The criterion then becomes

$$z_t > z_b \text{ or } \Omega < \left[\frac{\beta_0 - \beta_2}{\pi}\right] \rho \tag{5.108}$$

Because the difference $\beta_0 - \beta_2$ is proportional to ρ^{-2} (this will become clear in the discussion on the multimode interference coupler), the maximum taper angle will be larger when the waveguide is narrower. Therefore, the ideal taper design is parabolic.

2. Improving coupling efficiency to an optical fiber

   A typical monomodal optical fiber has a core diameter of 9 μm, has a small refractive index contrast between core and cladding layers ($\Delta n \approx 1\%$) and the mode is circular. The waveg-

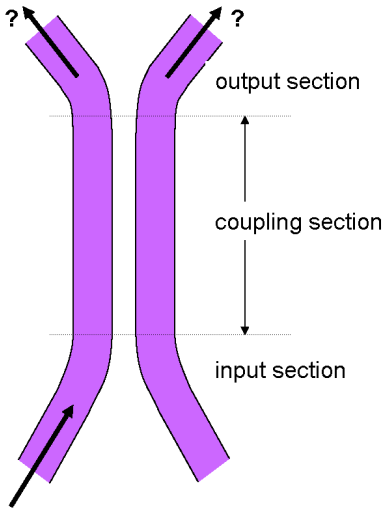

Figure 5.32: Sections of a directional coupler

uides fabricated in a III-V semiconductor material system typically are a few micrometer wide, have higher refractive index contrast and have non circular mode profiles.

The fundamental modes in the two systems strongly differ, therefore the coupling losses from fiber to waveguide will be high. A possible solution is the use of a taper structure. By narrowing the integrated waveguide (this can be done both transversally or vertically) the mode will expand and a better mode matching can be obtained, thereby reducing the coupling losses.

5.4.4 Directional coupler

The directional coupler was already treated in previous sections on coupled mode theory and supermode theory. In these cases always a longitudinally invariant waveguide structure was assumed. In reality, a directional coupler consists of a central section (in which the actual coupling takes place) and an input and output section. In many cases part of the optical power will already be exchanged between the waveguides in the input and output section where the waveguides are already in close proximity. This needs to be analyzed using the beam propagation method. The most important application of the directional coupler is the use as a 3dB coupler.

5.4.5 Multimode interference coupler

An alternative to the directional coupler is the use of a multimode interference coupler (MMI). The central part of an MMI is a broad multimode waveguide. Light can be injected in and coupled out of the multimode section through a number of input and output waveguides (figure 5.34). The operation principle of the device is based on the self imaging principle. This is a property of multimodal waveguides where an input field is reproduced in single and multiple images at periodic intervals along the propagation direction of the waveguide. In this way 1xN couplers can be realized, but also cross couplers and even couplers with an arbitrary coupling ratio.

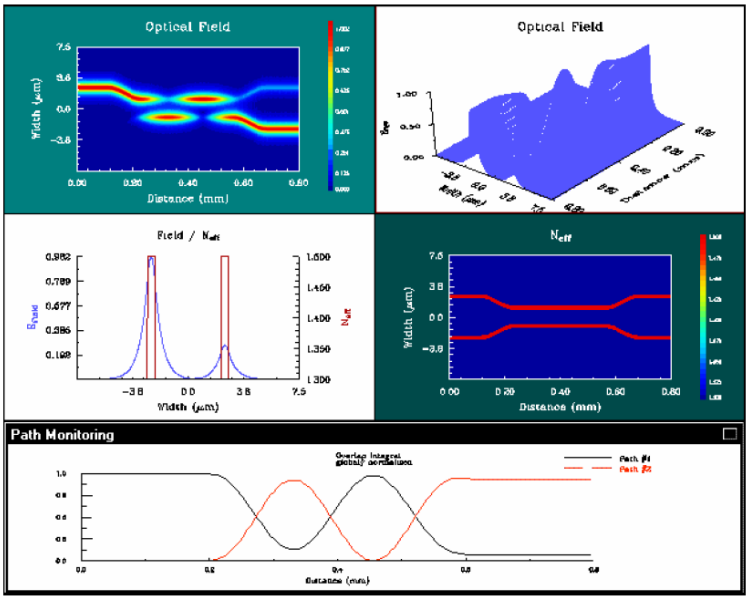

Figure 5.33: BPM simulation of a directional coupler. In the upper plots, the intensity profile and the electrical field profile is shown. The middle graphs show the field distribution at the exit of the directional coupler and the refractive index profile of the simulated directional coupler. In the bottom graph the power in both arms of the coupler is shown. The periodic power exchange is clear.

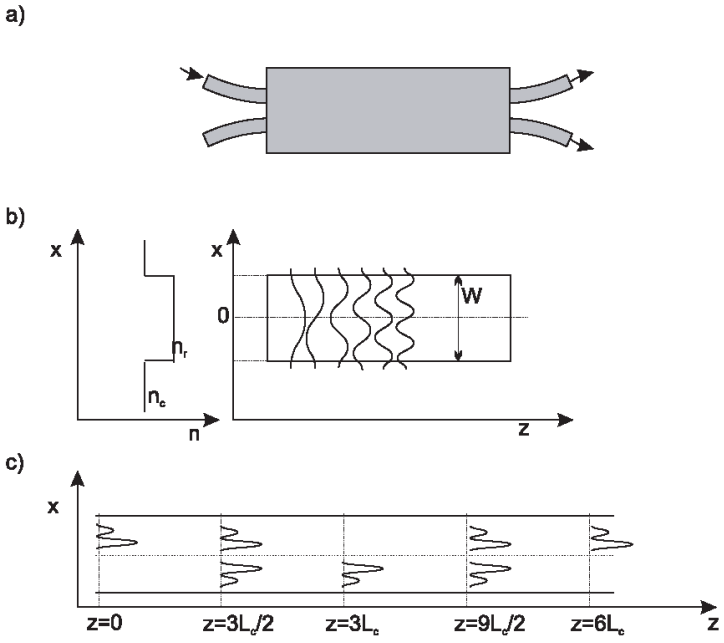

Figure 5.34: multimode interference coupler

To gain insight in the operation principle of the MMI, we will use the mode expansion and propagation theory. Lets consider the multimodal waveguide of width W which is depicted in figure 5.34b. An arbitrary input field $\Psi(x,0)$ of the MMI can be decomposed in the orthonormal eigenmodes ψ_i of the MMI.

$$\Psi(x,0) = \sum_{i=0}^{N-1} c_i \psi_i(x) \text{ with } c_i = \int \Psi(x,0)\psi_i(x)dx \tag{5.109}$$

In the expansion radiation modes have been neglected, which is acceptable as long as the width of the incident field $\Psi(x,0)$ is sufficiently small compared to the width of the MMI. After propagation over a distance z along the MMI the field becomes

$$\Psi(x,z) = \sum_{i=0}^{N-1} c_i \psi_i(x) e^{-j\beta_i z} = e^{-j\beta_0 z} \sum_{i=0}^{N-1} c_i \psi_i(x) e^{j(\beta_0 - \beta_i)z} \tag{5.110}$$

For the modes, the following approximation is made: we assume the shape and propagation constant of each mode to be given by these of the modes of a waveguide with an infinitely high refractive index contrast (field is zero at the edges of the waveguide)

$$\begin{aligned} &\psi_i(x) = \cos(k_{x,i}x) \text{ when } i \text{ is even} \\ &\psi_i(x) = \sin(k_{x,i}x) \text{ when } i \text{ is odd} \\ &k_{x,i} = \tfrac{(i+1)\pi}{W} \end{aligned} \tag{5.111}$$

For real waveguide structures this is only an approximation but in the case of high index contrast waveguides it is a very useful approximation.

As the lateral wave number $k_{x,i}$ and the propagation constant β_i are related through

$$k_{x,i}^2 + \beta_i^2 = k_0^2 n_r^2 \tag{5.112}$$

we find

$$\beta_i \approx k_0 n_r - \frac{(i+1)^2 \pi \lambda_0}{4 n_r W^2} \tag{5.113}$$

Therefore

$$\beta_0 - \beta_i = \frac{i(i+2)\pi\lambda_0}{4n_r W^2} = \frac{i(i+2)\pi}{3L_\pi} \tag{5.114}$$

with

$$L_\pi = \frac{\pi}{\beta_0 - \beta_1} = \frac{4n_r W^2}{3\lambda_0} \tag{5.115}$$

If we substitute this equation into equation (5.110) then we can write down the field in the MMI after a propagation distance L as (neglecting the common phase term)

$$\Psi(x,L) = \sum_{i=0}^{N-1} c_i \psi_i(x) e^{j\frac{i(i+2)\pi}{3L_\pi}L} \tag{5.116}$$

From this equation we can deduce some interesting properties of the MMI.

- $L = 6L_\pi$

  Then equation (5.116) becomes

  $$\Psi(x, 6L_\pi) = \Psi(x, 0) \tag{5.117}$$

  The image at this distance equals the input field

- $L = 3L_\pi$

  Because

  $$\begin{array}{l} \psi_i(-x) = \psi_i(x) \text{ when } i \text{ is even} \\ \psi_i(-x) = -\psi_i(x) \text{ when } i \text{ is odd} \end{array} \tag{5.118}$$

  we find

  $$\begin{aligned} \Psi(x, 3L_\pi) &= \sum_{i=0}^{N-1} c_i \psi_i(x) e^{j[i(i+2)]\pi} \\ &= \left[\sum_{i=0}^{N-1} c_i \psi_i(x) e^{j[i(i+2)]\pi}\right]_{i=even} + \left[\sum_{i=0}^{N-1} c_i \psi_i(x) e^{j[i(i+2)]\pi}\right]_{i=odd} \\ &= \left[\sum_{i=0}^{N-1} c_i \psi_i(x)\right]_{i=even} + \left[\sum_{i=0}^{N-1} -c_i \psi_i(x)\right]_{i=odd} \\ &= \left[\sum_{i=0}^{N-1} c_i \psi_i(-x)\right]_{i=even} + \left[\sum_{i=0}^{N-1} c_i \psi_i(-x)\right]_{i=odd} \\ &= \sum_{i=0}^{N-1} c_i \psi_i(-x) \end{aligned} \tag{5.119}$$

  This means that at a distance $3L_\pi$ the image is the input field, mirrored around the plane $x = 0$.

- $L = 3\frac{p}{2}L_\pi$ with p odd

  After some manipulation we find

  $$\begin{aligned} \Psi(x, \tfrac{p}{2}3L_\pi) &= \sum_{i=0}^{N-1} c_i \psi_i(x) e^{j[i(i+2)]p\frac{\pi}{2}} \\ &= \left[\sum_{i=0}^{N-1} c_i \psi_i(x)\right]_{i=even} + \left[\sum_{i=0}^{N-1} (-j)^p c_i \psi_i(x)\right]_{i=odd} \\ &= \tfrac{1+(-j)^p}{2}\Psi(x,0) + \tfrac{1-(-j)^p}{2}\Psi(-x,0) \end{aligned} \tag{5.120}$$

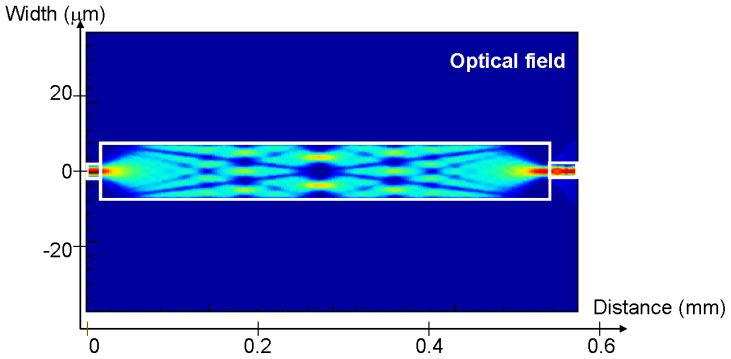

Figure 5.35: BPM simulation of a 1x1 MMI. The dimensions are 15x520 μm^2. On the figure the places where two folded (L/2), three folded (L/3,2L/3) and four folded images(L/4,3L/4) are formed, are clearly visible.

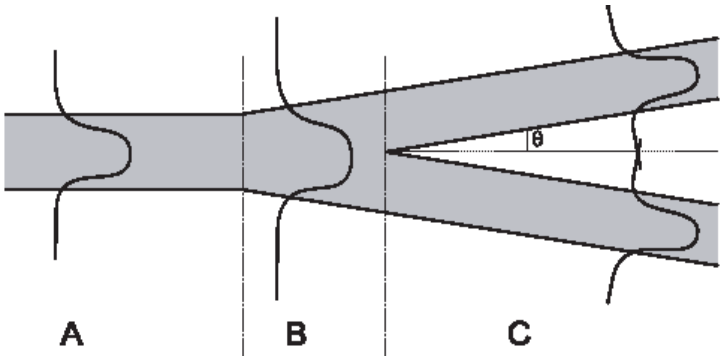

Figure 5.36: Y-junction

At this distance we find two images, of which one mirrored, both with amplitude $1/\sqrt{2}$. So an MMI with this length can be used as a 2x2 3dB coupler.

More general one can show that at the intermediate distances $L = 3\frac{p}{N}L_\pi$ (with p and N integer numbers without common divider) N multiple images are formed, with an amplitude of $\frac{1}{\sqrt{N}}$. This is illustrated in figure 5.34 and figure 5.35.

5.4.6 Y-junction

The Y-junction is composed of a single waveguide (section A), a taper (section B) and two branched waveguides (section C). An important parameter for the Y-junction is the junction angle θ. When the angle is sufficiently small, the fundamental mode will propagate without great losses in both exit waveguides in section C. This is called an adiabatic Y-junction. The standard Y-junction is designed to equally split the input power over both exit waveguides but it is also possible to design Y-junctions for different splitting ratios.

When we use the Y-junction in the other direction and excite only one branch of the Y-junction with the fundamental mode which propagates towards the junction, we can analyze what happens using the theory of supermodes.

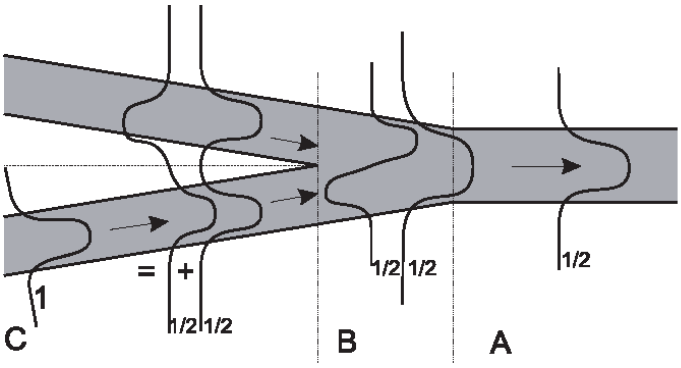

Figure 5.37: Y-junction used as a combiner

The mode propagating in the lower branch (with amplitude 1) of the Y-junction can be decomposed into the sum of the local symmetrical and anti-symmetrical supermode each carrying half of the power (amplitude $\frac{1}{\sqrt{2}}$). The symmetrical supermode will adiabatically transform to the fundamental mode of the exit waveguide, while the antisymmetric mode will be transformed into the first order mode. However, when the waveguides are monomodal, this part of the power will radiate. As both super modes carry half of the power, this half is lost. This property can also be explained based on reciprocity and symmetry of the Y-junction.

In conclusion, we can say that when we use an adiabatically designed Y-junction as a splitter, no losses occur. When used as a combiner no losses occur when both inputs are excited equally (both in phase and amplitude). This is the reciprocal situation of the use as a splitter. When only one of the inputs is excited, half of the power will be lost and when both inputs are excited equally but in antiphase all power will be lost (for monomodal waveguides).

5.4.7 Diffraction grating

The diffraction grating is analyzed in detail in the chapter on periodic structures. In the integrated version, the diffraction grating is mostly used as an dispersive element. In this way wavelength demultiplexers can be fabricated. Another application is the longitudinal mode selection in a laser cavity. By rotating the diffraction grating a wavelength tunable laser is made.

5.4.8 Phase modulator

Phase modulation in integrated waveguides can be achieved using different physical effects that influence the optical parameters of the material. The most important effects are the electro-optical effect, the thermo-optical effect and the influence of free carriers. All these effects create a change in the refractive index of the material which leads to a phase modulation given by

$$\Delta\phi = \frac{2\pi\Delta n_{eff}L}{\lambda} \tag{5.121}$$

in which L is the length of the waveguide and λ is the operation wavelength.

5.4.9 Amplifiers

An optical amplifier can be used to boost a signal in a waveguide. The amplifier can for example be used in front of a photodetector to reduce the required sensitivity of the photodetector or it can be used as an in line amplifier for long propagation distances. For this application both a doped optical fiber amplifier (EDFA: Erbium Doped Fiber Amplifier) or an SOA (Semiconductor Optical Amplifier) can be used. Sometimes the amplifier is used to amplify different signals (all at a different wavelength) at the same time. An important issue here is the crosstalk between different wavelength channel by saturation of the amplifier. A possible solution to this problem is the so called gain clamped amplifier, where the gain in the amplifier is kept constant.

5.5 Characterization of optical waveguides

Determining the performance of a passive optical waveguide circuit often consists of measuring the power transmission of the components. A typical measurement setup is shown in figure 5.38.

A light beam from a tunable laser (1) is focused on the right facet of the chip (5) using an optical fiber (2). The laser spot can be aligned to the waveguides using a micro translation stage (7,8,9) which is often actuated piezo-electrically (11). Part of the laser light will be coupled into the waveguides. The coupling efficiency is determined by the overlap integral of the laser spot and the waveguide modes. The coupling efficiency can be increased by using a lensed fiber (4). After transmission through the waveguide light will be coupled out through the left facet and collected using an objective lens (6) of which the focus is aligned with the left facet. Using an extra lens (13) this light is focused onto a power meter (15,16). A diafragm (14) makes sure only the light that comes from the waveguide is incident on the power meter. When we turn away the power meter it is possible to get a view of the spot with a camera (19,20,21). Polarization can be controlled by polarization control wheels at the input (3) and a polarization filter (12) at the output. Two other techniques to couple light in and out of a waveguide are prism coupling and grating assisted coupling. Grating assisted coupling uses a diffraction grating which is positioned on top of the waveguide to couple light into the chip.

When we assume that the coupling efficiency into the various waveguides on a chip is equal, we can this way do relative loss measurements, where different components are compared. Often the loss of the components are measured with the loss of a straight waveguide as a reference.

It is possible to eliminate the coupling efficiency by doing cut-back loss measurements. After a series of measurements the chip is cleaved in half and one half is used to redo the measurements. The difference between both measurements is the loss in the remaining part. It is clear that this measurement technique only works when the coupling efficiencies are equal for both parts.

An alternative way to measure the waveguide losses is the so called Fabry-Perot measurement technique. When we couple laser light into a waveguide, reflections occur at the facets which can be seen as partly reflecting mirrors. By adding the complex wave amplitudes of the subsequent reflections we can calculate the total transmitted power as

$$T = \frac{(1-R)^2\tau^2}{(1-\tau^2 R)^2 + 4\tau^2 R \sin^2(\beta L)} \text{ with } \tau^2 = e^{-\alpha L} \tag{5.122}$$

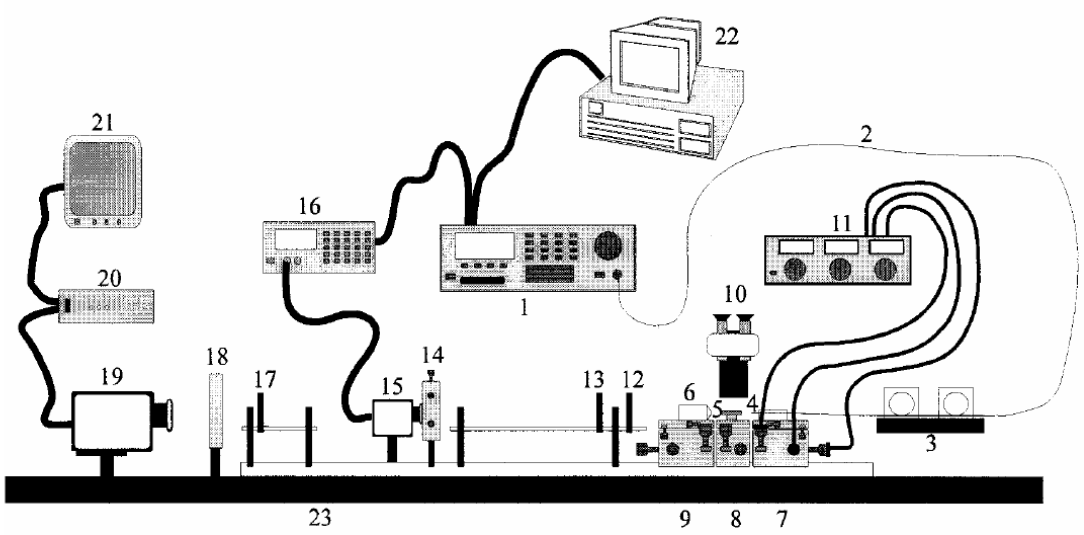

Figure 5.38: Measurement setup

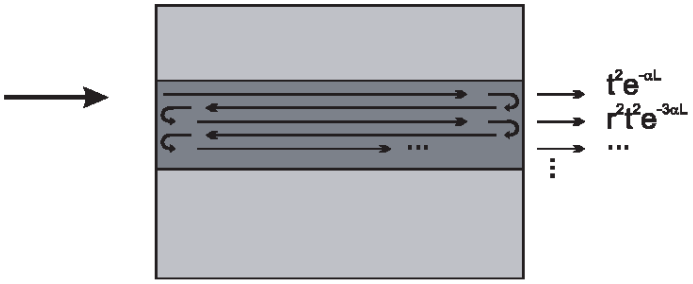

Figure 5.39: Fabry-Perot resonances in a waveguide

This transmission function is wavelength dependent (through the propagation constant β). When we calculate the ratio $\frac{T_{\max}}{T_{\min}}$ we find that

$$S = \frac{T_{\max}}{T_{\min}} = \frac{(1+\tau^2 R)^2}{(1-\tau^2 R)^2} \tag{5.123}$$

This way we can calculate the attenuation as

$$\alpha_{dB} = \frac{10}{L}(\log(R) - \log(\frac{\sqrt{S}-1}{\sqrt{S}+1}))[\mathrm{dB/cm}] \tag{5.124}$$

By measuring the transmitted power as a function of wavelength we can easily determine the ratio $\frac{T_{\max}}{T_{\min}}$. When we know the reflection coefficient R (typically 0.32 for waveguide in InP) we can determine the attenuation coefficient of the waveguide. For a correct measurement it is necessary however that only one mode is excited. In figure 5.40 two examples of this type of measurements are given. For the first measurement the determination of the ratio S is simple. For the second measurement an unambiguous measurement is impossible. There are many possible causes for

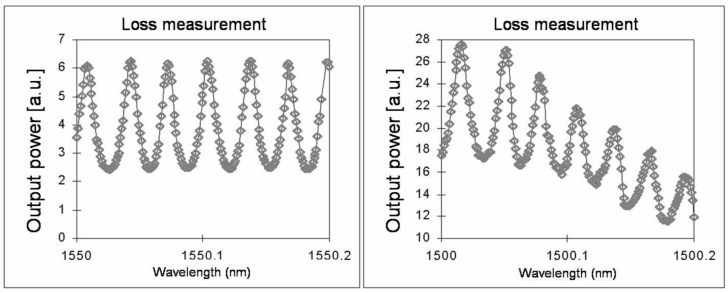

Figure 5.40: Fabry-Perot loss measurements

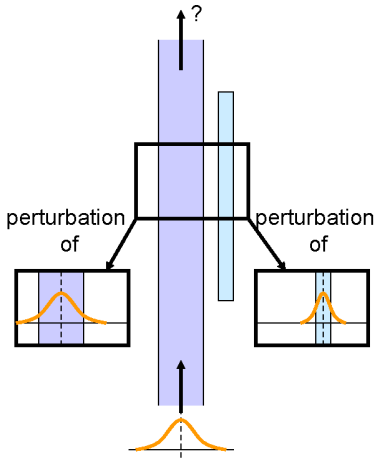

Figure 5.41: Double perturbed waveguide system

this problem: parasitic reflections in the measurement setup, vibrations, multimodal excitation, wavelength dependence of the focal distance between facet and objective lens...

5.6 Appendix

5.6.1 Calculation of the coupling coefficients $\kappa_{i,j}$ for a directional coupler

For the uncoupled waveguides with respective index profile $n_1(x)$ and $n_2(x)$ we can write

$$\begin{aligned} \frac{\partial^2\varphi_1(x)}{\partial x^2} + (k_0^2 n_1^2(x) - \beta_1^2)\varphi_1(x) = 0 \\ \frac{\partial^2\varphi_2(x)}{\partial x^2} + (k_0^2 n_2^2(x) - \beta_2^2)\varphi_2(x) = 0 \end{aligned} \tag{5.125}$$

For the field in the coupled waveguides we can write

$$\frac{\partial^2\Psi(x,z)}{\partial x^2} + \frac{\partial^2\Psi(x,z)}{\partial z^2} + k_0^2 n_{12}^2(x)\Psi(x,z) = 0 \tag{5.126}$$

If we propose following solution for $\Psi(x,z)$

$$\Psi(x,z) = C_1(z)\varphi_1(x)e^{-j\beta_1 z} + C_2(z)\varphi_2(x)e^{-j\beta_2 z} \tag{5.127}$$

in which C_1 and C_2 slowly vary with z so that we can assume

$$\left|\frac{\partial^2 C_i}{\partial z^2}\right| << \left|-j\beta_i \frac{\partial C_i}{\partial z}\right| \tag{5.128}$$

Substituting equation (5.127) into equation (5.126) and taking equation (5.128) into account, we find that

$$\begin{array}{c}\left[\frac{\partial^2\varphi_1(x)}{\partial x^2} + (k_0^2 n_{12}^2(x) - \beta_1^2)\varphi_1(x)\right] C_1 e^{-j\beta_1 z} - 2j\beta_1\varphi_1(x)\frac{dC_1}{dz}e^{-j\beta_1 z} \\ + \left[\frac{\partial^2\varphi_2(x)}{\partial x^2} + (k_0^2 n_{12}^2(x) - \beta_2^2)\varphi_2(x)\right] C_2 e^{-j\beta_2 z} - 2j\beta_2\varphi_2(x)\frac{dC_2}{dz}e^{-j\beta_2 z} = 0\end{array} \tag{5.129}$$

When we use equation (5.125), this becomes

$$\begin{array}{c}k_0^2\left[n_{12}^2(x) - n_1^2\right]\varphi_1(x)C_1 e^{-j\beta_1 z} - j2\beta_1\varphi_1(x)\frac{dC_1}{dz}e^{-j\beta_1 z} \\ +k_0^2\left[n_{12}^2(x) - n_2^2\right]\varphi_2(x)C_2 e^{-j\beta_2 z} - j2\beta_2\varphi_2(x)\frac{dC_2}{dz}e^{-j\beta_2 z} = 0\end{array} \tag{5.130}$$

When the eigenmodes are orthonormal

$$\beta_i \int \varphi_i(x)\varphi_j(x)dx = \delta_{ij} \tag{5.131}$$

we find that (by multiplying equation (5.130) with φ_1 and integrating over x):

$$\frac{dC_1}{dz}e^{-j\beta_1 z} = -j\kappa_{11}C_1 e^{-j\beta_1 z} - j\kappa_{12}C_2 e^{-j\beta_2 z} \tag{5.132}$$

and by multiplying equation (5.130) with φ_2 and integrating over x:

$$\frac{dC_2}{dz}e^{-j\beta_2 z} = -j\kappa_{22}C_2 e^{-j\beta_2 z} - j\kappa_{21}C_1 e^{-j\beta_1 z} \tag{5.133}$$

with

$$\begin{array}{l}\kappa_{11} = \frac{1}{2}k_0^2\int(n_{12}^2 - n_1^2)\psi_1^2 dx \\ \kappa_{12} = \frac{1}{2}k_0^2\int(n_{12}^2 - n_1^2)\psi_1\psi_2 dx \\ \kappa_{21} = \frac{1}{2}k_0^2\int(n_{12}^2 - n_2^2)\psi_1\psi_2 dx \\ \kappa_{22} = \frac{1}{2}k_0^2\int(n_{12}^2 - n_2^2)\psi_2^2 dx\end{array} \tag{5.134}$$

When

$$\begin{array}{l}X_1(z) = C_1(z)e^{-j\beta_1 z} \\ X_2(z) = C_2(z)e^{-j\beta_2 z}\end{array} \tag{5.135}$$

equation (5.132) and (5.133) become

$$\begin{array}{l} \frac{dX_1}{dz} = -j\beta_1 X_1 - j(\kappa_{11} X_1 + \kappa_{12} X_2) \\ \frac{dX_2}{dz} = -j\beta_2 X_2 - j(\kappa_{21} X_1 + \kappa_{22} X_2) \end{array} \tag{5.136}$$

These are the equations proposed by the coupled mode theory.